

X-ray Spectral Identification of Three Candidate Quiescent Low-Mass X-ray Binaries in the Globular Cluster NGC 6304

Sebastien Guillot¹, Robert E. Rutledge¹, Lars Bildsten², Edward F. Brown³,
George G. Pavlov⁴, and Vyacheslav E. Zavlin⁵

ABSTRACT

We report the search for low-mass X-ray binaries in quiescence (qLMXBs) in the globular cluster (GC) NGC 6304 using *XMM-Newton* observations. We present the spectral analysis leading to the identification of three candidate qLMXBs within the field of this GC, each consistent with the X-ray spectral properties of previously identified qLMXBs in the field and in other GCs – specifically, with a hydrogen atmosphere neutron star with radius between 5–20 km. One (XMMU 171433–292747, with $R_\infty = 11.6_{-4.6}^{+6.3}$ (D/5.97 kpc) km and $kT_{\text{eff}} = 122_{-45}^{+31}$ eV) is located within one core radius (r_c) of the centre of NGC 6304. This candidate also presents a spectral power-law component contributing 49 per cent of the 0.5–10 keV flux. A second one (XMMU 171411–293159 with $R_\infty = 10.7_{-3.1}^{+6.3}$ (D/5.97 kpc) km and $kT_{\text{eff}} = 115_{-16}^{+21}$ eV) is found well outside the optical core (at $\sim 32 r_c$) but still within the tidal radius. From spatial coincidence, we identify a bright 2MASS infrared counterpart which, at the distance of NGC 6304, seems to be a post-asymptotic giant branch star. The third qLMXB (XMMU 171421–292917 with $R_\infty = 23_{-10}^{+69}$ (D/5.97 kpc) km and $kT_{\text{eff}} = 70_{-20}^{+28}$ eV) is a low signal-to-noise candidate for which we also identify from spatial coincidence a bright 2MASS infrared counterpart, with 99.916 per cent confidence. Three qLMXBs from this GC is marginally consistent with that expected from the encounter rate of NGC 6304. We also report a low signal-to-noise source with an unusually hard photon index ($\alpha = -2.0_{-2.2}^{+1.2}$). Finally, we present an updated catalogue of the X-ray sources

¹Department of Physics, McGill University, 3600 rue University, Montreal, QC, H3A 2T8, Canada; guil-lots@physics.mcgill.ca, rutledge@physics.mcgill.ca

²Kavli Institute for Theoretical Physics and Department of Physics, Kohn Hall, University of California, Santa Barbara, CA 93106; bildsten@kitp.ucsb.edu

³Department of Physics and Astronomy, National Superconducting Cyclotron Laboratory, and the Joint Institute for Nuclear Astrophysics, Michigan State University, 3250 Biomedical Physical Science Building, East Lansing, MI 48824-2320; ebrown@pa.msu.edu

⁴The Pennsylvania State University, 525 Davey Lab, University Park, PA 16802; pavlov@astro.psu.edu

⁵Space Science Laboratory, Universities Space Research Association, NASA MSFC VP62, Huntsville, AL 35805; vyacheslav.zavlin@nasa.msfc.gov

lying in the field of NGC 6304, and compare this with the previous catalogue compiled from *ROSAT* observations.

Subject headings: Stars: neutron, X-ray: binaries, Globular clusters: individual: NGC 6304

1. Introduction

Transiently accreting low-mass X-ray binaries in quiescence (qLMXBs) produce useful constraints on physical models of the interiors of neutron stars. They were first discovered during the post-outburst periods of transient LMXBs Cen X-4 and Aql X-1, in which their faint emission ($L_X \sim 10^{32} - 10^{33} \text{ erg s}^{-1}$), interpreted as thermal black-body emission, had emission areas a factor of 100 smaller than implied by the projected area of a 10 km neutron star (NS). Further observations of Cen X-4 and new observations of 4U 2129+47 (Garcia 1994) and 4U 1608–522 (Asai et al. 1996b) confirmed these observational properties of the class of qLMXBs. At that time, it was suggested that some low-level mass accretion on to the compact object was required to power the observed luminosity, although what set the low-mass accretion rate (\dot{M}) was unclear (Van Paradijs et al. 1987; Verbunt et al. 1994).

An alternate explanation to low- \dot{M} accretion has become the dominant explanation for the quiescent emission of qLMXBs (Brown et al. 1998, BBR98 hereafter). An up to date summary of the theoretical developments of deep crustal heating and the related observations is provided here. In this different interpretation of the quiescent thermal emission, the luminosity is provided not by accretion on to the compact object, but by heat deposited in the neutron star crust by pressure-sensitive nuclear reactions. These reactions (Haensel & Zdunik 1990, 2003; Gupta et al. 2007; Haensel & Zdunik 2008, HZ08 hereafter), referred to as deep crustal heating (DCH), occur as matter is piled at the top of the neutron star surface, forcing the column below to greater density and electron Fermi energies. For example, beginning with pure ^{56}Fe at the top of the crust, the increasing electron Fermi energy induces electron capture at a density of $1.494 \times 10^9 \text{ g cm}^{-3}$; because of the odd-even staggering of nuclear masses, a second electron capture follows to produce ^{56}Cr and releases 0.041 MeV per accreted nucleon (HZ08). At a density $1.114 \times 10^{10} \text{ g cm}^{-3}$ the electron Fermi energy is again above threshold for capture on to ^{56}Cr , and ^{56}Ti is produced with an energy deposition of 0.036 MeV per accreted nucleon. This process continues, resulting in a series of electron captures, neutron emission, and pycnonuclear reactions, through the depth of the crust, until the matter reaches the density of undifferentiated equilibrium nuclear matter, at which point it is no longer constituted of differentiable nuclei. In doing so, this reaction chain deposits 1.9 MeV per nucleon, distributed throughout the crust (HZ08). Although the amount of heat deposited into the outer crust depends on the composition of nuclei produced by the fusing of accreted H and He (Gupta et al. 2007), the total amount of heat is dominated by neutron emissions and pycnonuclear reactions in the inner crust, giving a total heat deposition that is relatively insensitive to the nuclear history of the accreted matter (HZ08).

In a steady-state, these reactions give rise to a time-average luminosity, which is directly proportional to the time-average mass accretion rate (BBR98):

$$L = 9 \times 10^{32} \frac{\langle \dot{M} \rangle}{10^{-11} M_{\odot} \text{ yr}^{-1}} \frac{Q}{1.5 \text{ MeV/amu}} \text{ erg s}^{-1} \quad (1)$$

where Q is the average heat deposited in the NS crust per accreted nucleon. Of course, nuclear burning in the NS atmosphere will produce not pure iron, but a wide range of nuclei (Schatz et al. 1999, 2001); this has been shown (Haensel & Zdunik 2003) to possibly change Q to range between 1.1-1.5 MeV per accreted nucleon. Moreover, the uncertain time-scale for the pycnonuclear burning of ^{34}Ne (Yakovlev et al. 2006), which arises in the Fe-chain, leaves uncertain whether that reaction is followed, or some other reaction takes its place on a shorter time-scale, at slightly greater density. However, in the final analysis, the amount of heat Q deposited in the crust is roughly equal to the average mass defect of nuclei at the top of the crust (near densities $\approx 10^9 \text{ g cm}^{-3}$) with undifferentiated equilibrium nuclear matter at the bottom of the crust, near nuclear saturation density $2.6 \times 10^{14} \text{ g cm}^{-3}$ (HZ08).

Some qLMXBs exhibit significantly less photon luminosity than predicted by Eq. (1). In several cases, such as KS 1731–260 (Wijnands et al. 2001; Rutledge et al. 2002b; Cackett et al. 2006) and 1H 1905+000 (Jonker et al. 2007b) the long-term mass-transfer rate is not well constrained. For the accreting millisecond pulsar SAX J1808.4–3657, however, predictions of $\langle \dot{M} \rangle$ from the integrated fluence agree with predictions based on the orbital period and gravitational radiation losses (Bildsten & Chakrabarty 2001). For this system, the low quiescent luminosity is consistent with strong neutrino emission from the core, such as from nucleon or hyperon direct Urca processes (Heinke et al. 2007).

The energy source of the quiescent thermal luminosity aside, the thermal spectrum can be explained (BBR98) as due to a realistic neutron star hydrogen atmosphere model (Zavlin et al. 1996; Rajagopal & Romani 1996; Heinke et al. 2006), rather than a black-body approximation imposed in previous works. In the case of qLMXBs, the atmosphere has been accreted from the low-mass post-main sequence stellar companion (BBR98). When accretion shuts off, metals will settle gravitationally on a time-scale of \sim seconds (Bildsten et al. 1992), leaving a pure H-atmosphere. The emergent photon spectra of H atmosphere NSs is physically different – although parametrically similar – to that of blackbody thermal spectra (Zavlin et al. 1996), which dramatically changes the derived emission area radii from the $\lesssim 1 \text{ km}$ derived from the black-body assumption, to radii which are consistent with the entire area of the neutron star (Rutledge et al. 1999).

The DCH luminosity/H atmosphere spectral interpretation has been applied in the detection (and non-detections) of a large number of historically transient LMXBs, including: Cen X-4 (Campana et al. 2000; Rutledge et al. 2001b); Aql X-1 (Rutledge et al. 2001a) 4U 1608-522 (Rutledge et al. 1999); 4U 2129+47 (Rutledge et al. 2000); the transient in NGC 6440, SAX J1748–2021 (in’t Zand et al. 2001); X1732-304 in Terzan 1 (Wijnands et al. 2002); XTE J2123–058 (Tomsick et al. 2004); EXO 1747–214 (Tomsick et al. 2005); MXB 1659–29 (Cackett et al. 2006); 1M 1716–315

(Jonker et al. 2007a); 2S 1803–245 (Cornelisse et al. 2007); 4U 1730–22 (Tomsick et al. 2007); 1H 1905+000 (Jonker et al. 2007b).

The spectral analysis of qLMXBs with the H atmosphere interpretation leads to the determination of R_∞ , the emission radius (also called, the projected radius) of the neutron star. It differs from the physical radius by a factor g_r , the gravitational redshift:

$$R_\infty = \frac{R_{\text{NS}}}{g_r} = R_{\text{NS}} \left(1 - \frac{2GM_{\text{NS}}}{R_{\text{NS}} c^2} \right)^{-1/2} \quad (2)$$

The effective temperature is also affected by the gravitational redshift through the relation $T_{\text{eff}}^\infty = g_r T_{\text{eff}}$. A major uncertainty in accurate measurements of R_∞ remains the distance D to the system. While high signal-to-noise (S/N) X-ray spectra are capable of determining R_∞/D to statistical certainty, the 10–50 per cent systematic uncertainties in the distances to field sources directly contribute an additional 10–50 per cent uncertainty in R_∞ . The observational motivation for measuring R_∞ – placing observational constraints on the dense matter equation of state – requires measurements of R_∞ to ≈ 5 per cent accuracy, or better (Lattimer & Prakash 2004).

The observational solution is to discover new qLMXBs, the distances to which are known with greater certainty than the present group of field sources. Globular clusters (GCs) are the obvious place to search for these, as they host an over-abundance of LMXBs and their distances are precisely known or measurable. Historically, it was suggested that X-ray binary systems in GCs are formed by capture from the remnants of massive stars, i.e. neutron stars or black holes (Clark 1975). It was also noted that the ratio of X-ray sources to the surrounding stellar density is two orders of magnitude larger for GCs than for the Milky Way. For example, 12 out of ~ 100 known bright X-ray sources were lying within GCs while the population of GC represents only 10^{-4} of the total mass of the Milky Way (Hut et al. 1992). The encounter rate is related to the physical properties of GCs, so that the high stellar density in their core creates a propitious environment for large encounter rates (Verbunt 2002). Recently, a correlation was shown between the GC encounter rate and the number of hosted X-ray sources (Pooley et al. 2003) or between the GC encounter rate and the number of hosted accreting NS binary systems (Heinke et al. 2003c). In addition, cluster metallicity can play a significant role in the number of LMXBs in GCs (Kundu et al. 2002; Maccarone et al. 2003; Ivanova 2006; Sivakoff et al. 2007).

To date, only a handful of qLMXBs in GCs capable of producing high S/N X-ray spectra are known: in Omega Cen (Rutledge et al. 2002a; Gendre et al. 2003b); X5 and X7 in 47 Tuc (Heinke et al. 2003b, 2006); in NGC 6397 (Grindlay et al. 2001b); in M13 (Gendre et al. 2003a); in M28 (Becker et al. 2003); A-1 in M30 (Lugger et al. 2007); in M80 (Heinke et al. 2003a); in M55 and NGC 3201 (Webb et al. 2006). Others have been reported in the literature, but with lower S/N, or high values of N_H , which makes them significantly less useful for the primary motivation for searching for qLMXBs: providing measurements of R_∞ .

In each case, the qLMXB was identified by its X-ray spectrum alone, consistent with a H-atmosphere neutron star with radius of ≈ 10 km, without observation of an optical/IR counterpart,

or evidence of an historical X-ray outburst. In two cases – X5 in 47 Tuc (Edmonds et al. 2002) and Omega Cen (Haggard et al. 2004) – the optical counterpart of the binary was identified following the spectral classification, lending support to the assertion that X-ray spectral classification can identify qLMXBs.

Some qLMXBs also exhibit a power-law (PL) spectral component which dominates at photon energies above 2 keV. The first detection of such a component was made on the qLMXB Cen X-4 (Asai et al. 1996b, 1998), where the power-law contributes about 40 per cent of the 0.5–10 keV flux. Observations of 47 Tuc (qLMXBs X5 and X7) also showed weak power-law components (with photon index $\alpha = 2.6\text{--}3$) (Grindlay et al. 2001a). However, analysis of more sensitive observations concluded that PL components are not required (Heinke et al. 2003b). A more recently identified candidate qLMXB in 47 Tuc, has shown a power-law component that represents 65_{-22}^{+28} per cent of the 0.5–10 keV unabsorbed flux (Heinke et al. 2005). NGC 6440 have possible qLMXBs with significant PL components, but the large absorption in the direction of this GC prevents a justified classification of the X-ray sources due to the low photon flux where the thermal spectrum is dominant (in’t Zand et al. 2001). In general, qLMXBs in GCs display no or little power-law components while qLMXBs in the field more frequently tend to have a significant power-law component. A proposed interpretation relates the power-law emission as the residual of a recent accretion episode (Grindlay et al. 2001a). An alternate explanation evokes it to shock emissions via the emergence of a magnetic field (Campana & Stella 2000). However, neither of these two hypothesis are yet supported by observational evidence.

A program of short-integration *XMM-Newton* observations, using the pn camera, have been undertaken to survey GCs for qLMXB candidates, to increase the number of known qLMXBs in GCs. This paper reports the discovery of three candidate qLMXBs in NGC 6304 from spectral classification, XMMU 171433–292747, XMMU 171411–293159 and the low signal-to noise source, XMMU 171421–292917. These were found in short *XMM-Newton*/pn exposures targeted specifically for the discovery of examples of this class of objects. The organisation of this paper is as follows. In §2.1 and §2.2, the data reduction, the observations and the astrometric analysis are described. In §2.3, the spectral analysis of the detected sources are presented with detailed explanations for interesting sources, including a hard source with the photon index $\alpha = -2.0_{-2.2}^{+1.2}$. In §3, the observational properties of the three candidate qLMXBs are described. §4 covers a comparison with a previous observation of NGC 6304 with *ROSAT* (§4.1) and a comparison with the expected number of qNS in GCs (§4.2). Finally, §5 summarizes the results of this observation and concludes.

1.1. NGC 6304

The globular cluster NGC 6304 is located at the position R.A.=17h14m32.1s and Dec. = $-29^{\circ}27'44.0''$, (J2000) approximately 2.2 kpc from the galactic centre. Its integrated visual magnitude is $V = 8.22$ and it has a color excess $E(B - V) = 0.53$. NGC 6304 is moderately compact, with the core radius $r_c = 0.21'$, the half mass radius $r_{\text{HM}} = 1.41'$ and the tidal radius $r_t = 13.25'$.

It is a non core-collapse GC with a concentration $c = \log(r_t/r_c) = 1.80$ (assuming a King’s profile) and with a central luminosity density $\log(\rho_0) = 4.41 L_\odot \text{pc}^{-3}$. Finally, its metallicity [m/H] is -0.56, implying $Z = 0.00488$, where $Z_\odot = 0.0177$ was used (Montalbán et al. 2004). All properties come from the updated catalog of GCs (Harris 1996) or from a more recent work (Valenti et al. 2007). A more recent measurement of the cluster distance modulus, $(m - M)_0 = 13.88 \pm 0.03$, provides an heliocentric distance of 5.97 ± 0.08 kpc (Valenti et al. 2005).

2. Data Reduction and Analysis

2.1. Observation

The target was observed on 4 Sept 2006 using *XMM-Newton*. The three X-ray CCD cameras – MOS1, MOS2, and pn – were operating in imaging mode, with exposure times of 12618 sec, 12626 sec and 11037 sec, respectively. All exposures were made with the medium filter. The present analysis is focussed on the pn camera (Strüder et al. 2001), due to its greater sensitivity in the low photon energy range (0.5–2.0 keV) where qLMXBs are brightest. However, a drawback of the pn instrument is the multiple bad columns, which are accounted for during the analysis.

Data reduction was performed using *XMM-Newton* Science Analysis System v7.0.0, using standard analysis procedures. The command `epchain` performs all required steps for preliminary data reduction. The data were checked for proton flares, but the standard analysis found none. However, visual inspection of the exposure reveals a statistically significant background variability during the observation. Despite this, the full observed time interval has been used for this analysis. The spectral quality of the data is quantified using the task `epatplot`, as recommended before choosing the energy band ¹. Over the whole field, `epatplot` shows a significant discrepancy below 0.45 keV between the distribution of the various pattern events (single and double) as a function of energy and the expected curves, therefore excluding the use of this low energy band. The 0.5–10 keV spectral energy range was therefore chosen during the data reduction, the detection and the subsequent steps of the analysis. Only the event patterns recommended by the *XMM-Newton* Science team were used, that is, single and double patterns for the pn camera, and single, double and quadruple patterns for the MOS cameras. An exposure map was then created for source detection, which was performed with `wavdetect` from CIAO v3.4 (Fruscione et al. 2006). Using the pn data, a total of 11 sources were detected above a minimum `wavdetect` relative exposure of 0.2 (see Table 1 and Fig. 1). Other `wavdetect` parameters used are the wavelet scales (1.0 2.0 4.0 8.0) and the significance threshold (3×10^{-6}). Using the same detection parameters, 6 other sources are detected on a MOS1+MOS2 combined image, most of them being coincident with bad columns on the pn camera. The source ID numbers in this paper (from 0 to 10) are given by the default numbering of `wavdetect`, attributing the ID numbers by decreasing right ascension. The

¹From *XMM-Newton* Science Operations Center XMM-SOC-CAL-TN-0018, Guainizzi (2008)

additional MOS sources are labelled M1 to M6. The pn data was used to address the primary purpose of this observation. The source detected on the pn camera were spectrally fitted in order to identify candidate qLMXBs. For completeness and as a secondary objective of creating a catalog of X-ray sources in the field of NGC 6304, the sources detected on the MOS1+MOS2 image are reported in Table 2.

2.2. Astrometry

The astrometric positions given in Table 1 were derived in the following manner. Astrometry was first obtained using `wavdetect` with the pn data, the MOS1 data, and the MOS2 data, all separately. Comparing the relative astrometry for sources detected by each of these cameras, discrepancies are noticed in the relative astrometry for some sources. Sources #5, #6 and #9 relative distances from a reference source (see below) in the pn camera, compared with that from the MOS cameras, were not consistent with the statistical positional uncertainties. The observed inconsistencies seem to be due to bad columns on the pn camera, which are not accounted for in the `wavdetect` algorithm; thus `wavdetect` misestimates their positions in the direction opposite to the bad column (which is the direction of the discrepancy in all three cases).

Therefore, combining astrometric data from the pn and MOS1 cameras produced the X-ray astrometric positions of the detected sources. For most of the sources, the MOS1 data were used to deduce the positions of the sources. Some sources detected on pn, however, were not detected on the MOS1 camera (#2, #3, and #8). The astrometric positions of these sources are the pn position with a corrective offset calculated from the difference in the relative astrometry of the concerned source with source #1 on the two cameras. For example, $RA_3^{\text{MOS1}} = RA_3^{\text{pn}} + \Delta RA_{3\text{to}1}^{\text{pn}}$ is used to calculate the right ascension of source #3 as it would be on MOS1. The reference X-ray source is required to be detected on both cameras and not adjacent to a bad column. Only source #1 and #4 fulfil these conditions in the pn camera data, but source #4 was discarded since it is possible that it corresponds to unresolved multiple sources due to its presence in the core of NGC 6304.

Finally, an absolute astrometric correction – into the frame of the Two Micron All Sky Survey (2MASS) – is applied through the association of the X-ray source XMMU 171411–293159 with its counterpart 2MASS 17141152–2931594 (99.988 per cent confidence, see §3.2), shifting the X-ray positions by a change of -1.66 arcsec in R.A. and -1.02 arcsec in Dec. Previous to the frames alignment, the separation between the pn and the 2MASS sources, 1.77 arcsec is consistent with the absolute astrometric uncertainty of *XMM-Newton* (2 arcsec within $1\sigma^2$). The systematic uncertainty on the position, after the correction is 1.2 arcsec (1σ) (Jeffries et al. 2006). Also, the statistical uncertainty from the source detection (up to ~ 1 arcsec, depending on the source; see Table 1) should be added in quadrature to the systematic error to obtain the total uncertainty in

²from *XMM-Newton* Science Operations Centre XMM-SOC-CAL-TN-0018, Guainizzi (2008)

position.

2.3. Spectral Analysis

The X-ray counts for spectra are extracted using a radius of 25 arcsec around each source, accounting for 81 per cent of the total energy from the source at 1.5 keV. The background counts are extracted using an annulus centred at the position of the peak of the exposure map (that is, the image centre), and with an average radius equal to the distance between the source being analysed and the image centre. An annulus width of 40 arcsec is used for all sources, except those sources close to the centre (sources #4 and #5) for which a larger background area (100 arcsec circles) was extracted. Around each detected source, a circular area of 35 arcsec radius is excluded from the background annuli. A circular area of 35 arcsec excludes 87 per cent of the overlapping source counts (at 1.5 keV). In all cases, the sources contributes $\lesssim 30$ per cent of the Poisson uncertainty in the number of background counts – to the background regions. This choice of background area addresses mirror vignetting, which is the main cause of background variation across the field. At the source count rates encountered here, the effect of pile-up can be neglected. After the counts extractions, response matrices were created using `rmfgen` and `arfgen`, rather than using the predefined ones, in order to take into account the enclosed energies and the extraction radii.

A threshold of 70 counts above the background was imposed before considering the X-ray source for a full spectral analysis. Out of 11 detected sources, six satisfy this cut (ID #1, 4, 5, 6, 9 and 10) while the remaining five are too faint for a full spectral analysis (ID #0, 2, 3, 7 and 8). The counts were binned into energy bins between 0.5 and 10 keV with 25 counts per bins (or 20 counts per bins for sources with less than 100 counts in excess of the background).

Using XSPEC v12.3 (Arnaud 1996), the extracted spectra are fitted with a tabulated neutron star hydrogen atmosphere model (Zavlin et al. 1996). For this model, the radius is measured from the normalisation parameter $(R_\infty/(d/10 \text{ kpc}))^2$, assuming a distance $d = 5.97 \text{ kpc}$. If this model provides a statistically acceptable fit (Null hypothesis probability $\gtrsim 10^{-2}$) and values of R_∞ and kT_{eff} in the range of previously observed qLMXBs (see Table 4), 5–20 km and ~ 50 –150 eV respectively, then, the source is classified as a candidate qLMXB. The spectral parameters are then confirmed with a single-component model of neutron star hydrogen atmosphere included in XSPEC (NSA model: `nsa`, Zavlin et al. (1996)). Alternatively, two other NS atmosphere models are available in XSPEC: `nsagrav` (Zavlin et al. 1996) and `nsatmos` (McClintock et al. 2004; Heinke et al. 2006). When using any of those models, the mass is kept constant at $1.4 M_\odot$ and the model normalisation parameter $(1/d^2)$ is set assuming $d = 5.97 \text{ kpc}$. The `nsa` model contains a magnetic field parameter that is set to zero here while `nsagrav` and `nsatmos` assume non-magnetic atmospheres. In all cases, the models `nsa`, `nsagrav`, and `nsatmos` give consistent parameters. Regarding the surface gravity g , `nsa` has been implemented with a fixed value $g = 2.43 \times 10^{14} \text{ cm s}^{-2}$, `nsagrav` has been computed for a range $g = (0.1 - 10) \times 10^{14} \text{ cm s}^{-2}$ and `nsatmos` in the range $g = (0.63 - 6.3) \times 10^{14} \text{ cm s}^{-2}$

In the case where the NSA tabulated model provides a non-acceptable fit, a visual inspection and a F-test indicate whether a photon power-law should be added to the spectral fit. If a significant portion of the high energy tail is in excess of the NS atmosphere fit, a simple power-law is added. This is justified by the fact that qLMXBs sometimes display a hard power-law component which dominates the spectrum above 2 keV. If the fit is still not acceptable, the spectrum is fitted with a power-law alone and the flux is obtained. For low signal-to-noise ratio (S/N) source, the slope of the power-law is fixed at $\alpha = 1$ to estimate the flux. For all model fits, the photo-electric galactic absorption (the multiplicative model `wabs` in XSPEC) with a fixed value of $N_H = 0.266 \times 10^{22}$ atoms cm^{-2} (written $N_{H,22} = 0.266$ afterwards) at the position of the NGC 6304³ is included in the spectral fit.

A major technical problem arises during the spectral fitting with the `nsa` model, as well as with the `nsagrav` and `nsatmos` models. All three of them were implemented in XSPEC with restrictive parameter spaces. In particular, the radius parameter space is defined only between 5 km and 20 km for `nsa`, between 6 km and 45 km for `nsatmos` and between 6 km and 30 km for `nsatmos`. In this case, while the best-fit may be statistically acceptable, and the parameter values obtained are consistent with those expected for a qLMXB, the parameter uncertainty range is greater than that tabulated in the XSPEC models and the uncertainty calculation fails due to zero diagonal components in the parameters matrix. The consequence of the imposed cut off in the parameter space would be a misrepresentation of the parameter uncertainties, preventing any conclusions to be drawn from the spectral fit. In those cases, the tabulated model (Zavlin et al. 1996) and the parameters resulting from the fit are used, since they do not suffer from this constraint. In all cases of identified qLMXBs, the MOS1 and MOS2 spectra are extracted in a similar manner as described above, and used those to perform a simultaneous fit. This procedure reduced the uncertainties on the temperature and radii of the candidate qLMXBs, by up to fifty per cent.

The results of this spectral analysis are given in Table 3. The following subsections present two sources that are not candidates qLMXBs but which were above the signal-to-noise cut-off for spectral analysis and the results of the spectral fitting of source #8, an X-ray source with an extremely hard photon power-law. Finally, the spectral results for the three qLMXB candidates are described in §3.

2.3.1. XMMU 171516-292224 - Source #0

This source, located far from the optical centre of the GC ($\sim 52r_c$), is not spectrally consistent with a qLMXB at the distance of NGC 6304. Using the tabulated H-atmosphere model with a fixed N_H ($N_{H,22} = 0.266$), gives a non acceptable fit (χ^2_ν/dof (prob.) = 3.0/12 (3×10^{-4})) to the spectrum of the source. Allowing N_H to vary provides an acceptable fit χ^2_ν/dof (prob.) = 1.2/11 (0.28) with

³From <http://cxc.harvard.edu/toolkit/colden.jsp> using the NRAO data Dickey & Lockman (1990)

$N_{H,22} = 18.2_{-9.4}^{+11.7}$ but the resulting projected radius $R_\infty = 1.3_{-0.22}^{+0.25}$ km excludes a possible quiescent neutron star interpretation since the value is significantly smaller than previously measured for such objects.

A power law spectral model is therefore chosen to characterize the X-ray emission and it is found that with $N_{H,22} = 0.266$, the photon index is $\alpha = -0.24_{-0.82}^{+0.62}$ for which the statistic is χ_ν^2/dof (prob.) = 1.0/12 (0.45). If the absorption is chosen to be a free parameter, the fit is still statistically acceptable (χ_ν^2/dof (prob.) = 0.84/11 (0.60)) with the parameters $N_{H,22} = 1.6_{-6.2}^{+1.6}$ and $\alpha = 0.3_{-1.0}^{+2.4}$. Finally, a search for a possible 2MASS counterpart found no source within 3 sigma of the position of source #0.

2.3.2. XMMU 171453-292436 - Source #1

Using the H-atmosphere tabulated model, a non acceptable fit with χ_ν^2/dof (prob.) = 2.47/15 (0.001) is obtained when N_H is fixed at $N_{H,22} = 0.266$. On the other hand, as N_H is allowed to vary, the best fit (χ_ν^2/dof (prob.) = 0.98/14 (0.47)) projected radius $R_\infty = 0.28_{-0.08}^{+0.11}$ km excludes the qLMXB classification for this source. In addition, the best-fit (with fixed N_H) exhibits an excess high energy tail, suggesting an additional power-law component at high energies. Adding a power-law component to the assumed spectrum results in a dominating power-law (~ 100 per cent of the source 0.5–10 keV flux) of slope $\alpha \sim 0.5$. The NS atmosphere component is therefore abandoned and the spectral fit is restricted to a single power-law for which the best-fit photon index is $\alpha = 0.52_{-0.35}^{+0.34}$ with a value χ_ν^2/dof (prob.) = 0.96/15 (0.5) in the case where $N_{H,22} = 0.266$. However, as $N_{H,22} = 2.3_{-1.6}^{+1.9}$, the photon index is $\alpha = 1.7_{-0.9}^{+1.4}$ for which χ_ν^2/dof (prob.) = 0.65/14 (0.82).

2.3.3. XMMU 171417-293222 - Source #6

The NSA tabulated model produces an acceptable fit (χ_ν^2/dof (prob.) = 1.3/12 (0.21) for $N_{H,22} = 0.266$ and χ_ν^2/dof (prob.) = 1.3/11 (0.21) for $N_{H,22} = 20.8_{-20.8}^{+108}$) but in both cases the obtained parameters ($R_\infty < 1$ km and $kT_{\text{eff}} \sim 0.5$ keV) are not in accordance with expected values for NSs in quiescence. Also, visual inspection of the fitted spectrum indicates a significant high energy tail. The fit of the model (tabulated model+PL) is also statistically acceptable (χ_ν^2/dof (prob.) = 0.96/10 (0.48)) but, similarly to source #1, ~ 100 per cent of the unabsorbed flux comes from the power-law component. The single power-law model ($\alpha = 0.64_{-0.90}^{+0.87}$) provide a statistically acceptable fit (χ_ν^2/dof (prob.) = 0.75/12 (0.70)). The spectrum fit with a fixed slope ($\alpha = 1$) results in an almost unchanged χ_ν^2 statistic (χ_ν^2/dof (prob.) = 0.75/13 (0.71)). Finally, as both the absorption and the photon index are allowed to vary, the best fit parameters are $\alpha = 0.45_{-0.8}^{+1.0}$ and $N_{H,22} \leq 0.9$ for χ_ν^2/dof (prob.) = 0.78/11 (0.66).

2.3.4. XMMU 171413–293415 - Source #8

Even though it is one of the faint sources, XMMU 171413–293415 is interesting since a single power-law spectral model suggests a spectrally hard source. As N_H is kept fixed at $N_{H,22} = 0.266$, the best fit photon index $\alpha = -2.0_{-2.2}^{+1.2}$ with χ^2_{ν}/dof (prob.) = 1.726/7 (0.10) implying an unabsorbed flux $F_X = 2.8 \times 10^{-13} \text{ erg cm}^{-2} \text{ s}^{-1}$. When the absorption is a free parameter, the photon index, $\alpha = -2.1$, is similar to the case where N_H is fixed, but the large χ^2_{ν} value, χ^2_{ν}/dof (prob.) = 2.02/6 (0.06), greater than 2 does not allow for error estimation.

Most of the counts are in the range 5–10 keV (Fig. 2). The 5–10 keV light curve (100 sec bins) exhibits no variability (Fig. 3). The average number of counts per bin is 1.12, and 0.78 counts are expected on average due to the background. So, the average number of source counts is 0.43. A bin with 5 counts is found and the Poisson probability of finding a bin with such a peak in the lightcurve with a mean of 1.21 is 2.2 per cent. Also, the peak does not represent a variation by more than a factor of 10 of the mean number of source counts. The spectrally hard source is consistent with constant emission throughout the duration of the observation, to within a factor of < 10 in any 100 second bin. This excludes a source type such as an X-ray flash or soft gamma-ray repeater (SGR), which tend to be spectrally hard in the 1–10 keV energy band as exhibited by this object, but exhibit transient emission of duration \sim few msec, to \sim 100 sec. No detailed variability analysis can be performed due to the highly variable background. In conclusion, no variability is detected on a $\lesssim 100$ sec time-scale.

To confirm the existence this source, the MOS2 camera data were used (the CCD 6 on MOS1 containing source #8 was inoperative during the observation). The same data reduction as described for the pn camera and the same detection procedure is performed. As explained before, the data quality of the MOS camera is much better than the pn but its sensitivity is not as good as the pn camera. On MOS2, a total of 73 counts are detected within 25 arcsec of the expected position of source #8, with 2254 ± 47.5 counts in the background annulus. From the scaling factor between the source and the background areas, 50.3 ± 1.1 background counts are expected within the source extraction region. Therefore, there is an excess of 22.7 ± 8.6 counts, corresponding to a low-significance detection (2.6σ); the corresponding flux, assuming a power-law of slope $\alpha = -2.0$, is $2.6 \times 10^{-13} \text{ erg cm}^{-2} \text{ s}^{-1}$ using the tool *webPIMMS*⁴, which is consistent with the $2.8 \times 10^{-13} \text{ erg cm}^{-2} \text{ s}^{-1}$ value measured from the pn spectrum. Cross identification with the 2MASS and Digital Sky Survey (DSS) catalogues did not exhibit any counterparts in the J and B bands within 3σ of the X-ray position, respectively.

While the low signal-to-noise ratio of this detection ($S/N = 4.0$) does not permit any detailed analysis of this source, it is unusually spectrally hard for an object detected in the 0.5–10 keV band. Examination of the unfiltered event list (i.e. including all event patterns) finds no unusual number of rejected events, which does not support an interpretation of the source detection as due to a

⁴available at <http://heasarc.nasa.gov/Tools/w3pimms.html>

particle impact on the detector or an instrumental effect such as a transient thermal excess on the detector. Higher sensitivity observations are required to better characterize this source.

3. Candidate qLMXBs

This section presents the spectral analysis of sources which, on the basis of this spectral analysis, are candidate qLMXBs.

3.1. XMMU 171433–292747 - Source #4

This X-ray source, located near the centre of the cluster, has the highest count rate among the sources in the field (43.8 ± 2.8 cts ks⁻¹).

The fit with the tabulated NS atmosphere model is statistically acceptable (χ^2_ν/dof (prob.) = 1.24/21 (0.20)) and is producing values for R_∞ and kT_{eff} in the range expected for a NS in quiescence. However, there exists a systematic excess of counts above the best-fit model at photon energies larger than 3 keV suggesting an additional high-energy spectral component, which are accounted for by the addition of a power-law. The low probability value of the F-test (prob=0.014) suggests that adding a power-law component better describes the data than the absorbed H-atmosphere alone. The best-fit (tabulated) NSA model with the power-law component has a fit statistic χ^2_ν/dof (prob.) = 0.69/19 (0.83) (see Fig. 4). Also, $R_\infty = 8.1^{+8.3}_{-2.5}$ km and $kT_{\text{eff}} = 127^{+31}_{-29}$ eV with $N_{H,22} = 0.266$. These values are in agreement with other known qLMXBs (Table 4). However, when leaving the absorption free $N_{H,22} = 0.51^{+0.18}_{-0.30}$ for this model, the fit is acceptable (χ^2_ν/dof (prob.) = 0.63/18 (0.88)) but the radius is larger than expected for a neutron star, $R_\infty = 47^{+190}_{-21}$ km.

The fit with fixed N_H is confirmed with a `nsa+powerlaw` model, for which the χ^2_ν statistic is χ^2_ν/dof (prob.) = 0.83/19 (0.67). The radius ($R_{\text{NS}} = 8.3^{+9.2}_{-3.0}$ km) and temperature ($kT_{\text{eff}} = 117^{+59}_{-44}$ eV) suggests a candidate qLMXB since the X-ray spectrum is consistent with the thermal spectrum of observed qLMXBs at the distance of NGC 6304. The slope of the power-law is $\alpha = 1.5^{+0.9}_{-0.8}$ and this component of the model contributes to 49 per cent of the total unabsorbed 0.5–10 keV flux of the source. A simultaneous fit using the MOS1, MOS2 and pn spectra improved the statistics (χ^2_ν/dof (prob.) = 0.85/42 (0.75)) and the uncertainties on the parameters. The radius and temperature of this candidate qLMXB are now $R_{\text{NS}} = 8.1^{+4.2}_{-2.4}$ km and $kT_{\text{eff}} = 122^{+31}_{-45}$ eV, and the photon index is $\alpha = 1.2^{+0.7}_{-0.8}$. The value R_{NS} is converted to R_∞ assuming a $1.4 M_\odot$ neutron star using Eq. 2: $R_\infty = 11.6^{+6.3}_{-4.6}$ km.

The absence of significant intensity variability over the time scale of the observation further supports the classification of this source as a qLMXB. Moreover, the luminosity is consistent with being the same as that observed during the *ROSAT* observation 14 yr earlier (see Table 5 and section 4.1). This is consistent with the expected stable thermal luminosity from a qLMXB on this

time-scale (BBR98, Ushomirsky & Rutledge 2001).

The possibility of two unresolved sources – one spectrally hard and one spectrally soft – is investigated by separating the data into soft (< 1.5 keV) and hard (> 1.5 keV) images and performing a source detection as described in Sec. 2.1. Source #4 is detected in both bands, 24.6σ and 4.5σ significances in the soft and hard bands respectively (the 1.5 keV division was selected as the lowest possible photon energy which provides a significant source detection – a cutoff of 2.0 keV finds no source with $> 3\sigma$ significance above 2.0 keV). A positional offset of 3 ± 0.9 arcsec is measured between the positions of the source in the two images, which is marginally consistent with a single source. It is possible that an unresolved hard X-ray source lie close to the candidate qLMXB and was interpreted as a high energy tail in the spectrum of source #4. In other words, it is not possible to exclude that higher spatial resolution observations may resolve XMMU 171433–292747 into multiple X-ray sources.

3.2. XMMU 171411–293159 - Source #9

3.2.1. Spectral Characterisation of the X-ray source

The fit with the tabulated NS atmosphere model with fixed N_H is statistically acceptable and does not require an additional power-law (Fig. 5). The χ^2_ν statistic is χ^2_ν/dof (prob.) = 1.29/16 (0.20), the projected radius is $R_\infty = 15.3^{+15.5}_{-5.2}$ km and the effective temperature is $kT_{\text{eff}} = 100^{+24}_{-19}$ eV. Letting the absorption vary also gives a statistically acceptable fit (χ^2_ν/dof (prob.) = 1.38/13 (0.16)) with the following parameters: $N_{H,22} = 0.20^{+0.37}_{-0.20}$, $R_\infty = 9.8^{+31}_{-0.9}$ km and $kT_{\text{eff}} = 115^{+91}_{-61}$ eV, all statistically consistent with the fit with a fixed absorption.

The confirmation with any of the models `nsa`, `nsagrav` and `nsatmos` fails because the fit, while statistically acceptable, produces error regions larger than the allowed parameter space in XSPEC. It is therefore not possible to derive the uncertainty region for the spectrum of XMMU 171411–293159 using these models. In consequence, the results of the tabulated model show that the model fit is consistent with the thermal spectrum of a qLMXB at the distance of the NGC 6304. Moreover, no significant variability over the time-scale of the observation is observed, with weak constraints. To better improve the statistics and uncertainties, the MOS1, MOS2 and pn spectra are fitted simultaneously. The resulting fit is statistically acceptable (χ^2_ν/dof (prob.) = 1.20/31 (0.21)) and the obtained parameters are: $kT_{\text{eff}} = 115^{+21}_{-16}$ eV and $R_\infty = 10.7^{+6.3}_{-3.1}$ km. Those values for XMMU 171411–293159 are reported as a candidate qLMXB in Tables 3 and 4.

For completeness, additional spectral fits are provided. First, A single power law with fixed absorption ($N_{H,22} = 0.266$) gives an acceptable fit (χ^2_ν/dof (prob.) = 1.37/14 (0.16)) with a soft photon index, $\alpha = 3.51^{+0.40}_{-0.37}$. Leaving the galactic absorption N_H free $N_{H,22} = 0.57^{+0.44}_{-0.17}$, a steeper power-law is found $\alpha = 5.0^{+2.4}_{-1.5}$ with a χ^2_ν -statistic χ^2_ν/dof (prob.) = 1.28/13 (0.21). A single temperature Raymond-smith plasma fit with variable absorption and solar metallicity also produces

an acceptable fit (χ^2_{ν}/dof (prob.) = 1.03/13 (0.42)) with the following best-fit parameters: $N_{H,22} = 0.19^{+0.14}_{-0.15}$ and $kT_{\text{eff}} = 0.76^{+0.26}_{-0.17}$ keV. Thus, the spectrum of this (highest S/N) X-ray source is consistent with other spectral interpretations; however, such a steep power-law (either $\alpha = 3.5$, or $\alpha = 5.0$) is usually interpreted as indicating a thermal spectrum.

As mentioned above, the pn camera suffers bad pixel quality. Two of the detected sources (#6 and #9) are overlapping with bad columns. So for XMMU 171411–293159, an additional analysis using the MOS 1 and 2 cameras is performed. Source #9 is detected with a signal-to-noise ratio of 17.7 and 17.6 for MOS1 and MOS2 respectively. Using the tabulated model, the spectral fits of the MOS1 and MOS2 data and the simultaneous spectral fit of the MOS1, MOS2 and pn data are all statistically acceptable and give results similar to the ones obtained from the pn camera alone.

3.2.2. Search for an IR counterpart

Using the online 2MASS Point Source Catalogue (2MASS–PSC), a probable IR counterpart (2MASS 17141152–2931594; $m_J = 8.796(22)$, $m_H = 8.361(18)$, $m_K = 8.213(20)$, where the numbers in parenthesis are the 1σ uncertainties in the preceding digits) is found located at a distance of 1.77 arcsec (before astrometric correction to the 2MASS frame). For comparison, there are 6 stars of this magnitude or brighter in an annulus ($r_{\text{in}} = 4.5'$ and $r_{\text{out}} = 8'$) about the centre of the GC. The probability that another source as bright or brighter lies as close or closer to our X-ray source is 0.012 per cent. Therefore, the association between XMMU 171411–293159 and 2MASS 17141152–2931594 is identified on the basis of spatial proximity, with 99.988 per cent confidence. Also, the USNO-B1.0 catalogue (Monet et al. 2003) lists an object at this location (separated by <0.5 arcsec) with $B = 11.66$ and $B = 11.28$. The two different magnitudes may indicate time variability of the counterpart.

A photometric study of NGC 6304 finds an observed $V = 10.65$ for 2MASS 17141152–2931594 (S. Ortolani, private communication, 2008); this is about 3 magnitudes above the observed tip of the red giant branch (Ortolani et al. 2000) (see Fig 7), however, due to saturation of the CCD, the photometry of very bright stars, like this counterpart, was not performed – thus, objects as bright as this were not included in the published data⁵. Inspecting by eye a V -band exposure of NGC 6304 (S. Ortolani, private communication, 2008) shows that ~ 15 – 20 such saturated stars were not included in the BV photometric study of this GC.

The color-magnitude diagrams (Figs. 6 & 7) containing theoretical isochrones for ages in the range $t = 10^{8.55} - 10^{10.15}$ yr and metallicity $Z=0.00488$ (Marigo et al. 2008) show that the optical counterpart is consistent with a post-asymptotic giant branch (post-AGB) star, both in V and J bands. Even if the time scale of this stage is short, finding such an object in a GC is not completely

⁵The photometry for 2MASS 17141152–2931594 was performed by S. Ortolani from a separate shorter (10 sec) V -band exposure

unexpected. Based on previous work, 16 planetary nebulae (PN) are expected to be found in the GCs system of the galaxy (Jacoby et al. 1997). This corresponds to 6.7×10^{-7} PN L_{\odot}^{-1} , using the total luminosity of the GCs system, $\sim 2.4 \times 10^7 L_{\odot}$ (Secker 1992). Using the estimated mass of NGC 6304 (Gnedin et al. 2002)⁶ and the average mass-to-light ratio of GCs, $M/L = 1.7$ (Caputo 1985), 0.25 PNs are expected in this cluster. Since the lifetime of a PN, $\sim 10^4$ yr (Jacoby et al. 1997), is comparable to that of a post-AGB object, $\sim 10^3 - 10^4$ yr (Siódmiak et al. 2008; Bloeker 1995), finding one post-AGB star in NGC 6304 is not completely unexpected, and is consistent with the object classification.

To obtain the bolometric luminosity of 2MASS 17141152–2931594 at the distance of NGC 6304, the reddening $E(K - V)$ is first calculated using $E(K - V)/E(B - V) = -2.744$ (Rieke & Lebofsky 1985), where $E(B - V) = 0.53$ for NGC 6304. The intrinsic color is $(V - K)_0 = (V - K) + E(K - V) = 2.38 - 1.45$. Using bolometric corrections obtained from 2MASS photometry (Masana et al. 2006) as a function of $(V - K)_0$ and of the average metallicity of the cluster $[m/H] = -0.56$ (Valenti et al. 2007), the K -band bolometric correction is $BC_K = 0.892$. Using a K -band extinction correction, $A_K = 0.36 E(B - V)$ (Fitzpatrick 1999), $m_{\text{bol}} = m_K - A_K + BC_K = 8.914$ is finally calculated to be able to work out the bolometric luminosity. Taking a zero absolute bolometric magnitude $M_{\text{bol}} = 0$ star to correspond to a luminosity of 2.97×10^{35} erg s^{-1} (Harwit 2006) and the distance modulus, the absolute bolometric magnitude is $M_{\text{bol}} = -4.96$, for a bolometric luminosity of 2.9×10^{37} erg s^{-1} .

As a check on the value calculated for the bolometric luminosity, a less precise method of estimation is used (since it does not take into account effects of realistic atmospheres, such as limb darkening), by fitting a blackbody curve to the unabsorbed photometry in $BVJHK$ bands. For a blackbody source at the distance of NGC 6304, this resulted in a best fit ($\chi^2/\text{dof} = 5.8$, for 3 dof) of $R = 46 \pm 1.0 R_{\odot}$, $T_{\text{eff}} = 6620 \pm 140$ K, for a total luminosity of $L = 4\pi R^2 \sigma T_{\text{eff}}^4 = 1.4 \times 10^{37}$ erg s^{-1} ; this is a factor of $\times 2.1$ below that derived through the more precise method, which may be indicative of the systematic uncertainties in approximating the total luminosity using a blackbody fit to the $BVHJK$ data, but which is regarded as consistent with the more precise BC_K calculation method.

3.2.3. Examining the Hypothesis that XMMU 171411–293159 is a Foreground Star

The hypothesis that 2MASS 17141152–2931594 is a field dwarf star is investigated. First, this star (TYC 6824-713) is listed in the Tycho-2 catalog (issued from a re-analysis of the Hipparcos data) providing proper motion, but no parallax information (?). The proper motion observed for this star is -6.6 ± 2.8 milli-arcseconds per year, marginally consistent (at 2.4σ) with a zero proper motion, as would be expected for a cluster member. This does not resolve the possible cluster membership versus the foreground star hypothesis.

If reddening dust is distributed uniformly between the observer and NGC 6304, the source,

⁶Online data at <http://www.astro.lsa.umich.edu/~ognedin/gc/vesc.dat>

assuming it is a main-sequence star, is most consistent with an $M_V = 4.4$ object at a distance 170 pc, with $E(B - V) = 0.03$, based on the absolute magnitude M_V and color $B - V$ values of stars in the Hyades (de Bruijne et al. 2001).

For main-sequence stars, the typical X-ray to bolometric flux ratio seems to reach an upper limit at 10^{-3} (Vilhu & Walter 1987). For the association XMMU 171411–293159/2MASS 17141152–2931594, the X-ray to bolometric flux ratio is of the order of $\sim 10^{-5}$, therefore consistent with a main-sequence foreground star.

In a $B - V$ vs. $J - K$ color-color diagram (Fig. 8), XMMU 171411–293159 lies marginally off the main-sequence (by between 2 and 3 σ) for a wide range of metallicities ($Z = 0.0001 - 0.03$), lying closest to stars in the mass range $0.7-0.9 M_\odot$, depending on metallicity, according to theoretical isochrones (Marigo et al. 2008). This marginal result from the color-color diagram does not definitively exclude the possibility that the star is in the foreground.

The X-ray emission from dMe stars is spectrally comparable to those of RS CVn (Singh et al. 1996). Typically, RS CVn exhibit a two-temperature Raymond-Smith plasma model (Dempsey et al. 1993). Since the number of counts are not sufficient for such a fit with all parameters left free, the spectrum of XMMU 171411–293159 is fitted twice with a two-temperature Raymond-Smith plasma model keeping the high temperature component fixed at the lowest ($kT_2 = 0.93$ keV) and highest value ($kT_2 = 3.45$ keV) from the sample of RS CVn (Dempsey et al. 1993). The metallicities are also held fixed at the solar value, $Z = 0.0177$. The normalization of the Raymond-Smith model in XSPEC model provides the emission measure ($EM = \int n_e n_H dV$), a distance dependent value. The best fit parameters for those two statistically acceptable fits are $N_{H,22} = 1.3_{-0.4}^{+0.6}$, $kT_1 = 0.11_{-0.04}^{+0.04}$ keV, $EM_1 = 1.9_{-1.8}^{+11.2} \times 10^{60} \text{ cm}^{-3}$ and $EM_2/EM_1 = 1_{-1}^{+5} \times 10^{-5}$ for the first fit corresponding to $kT_2 = 0.93$ keV and $N_{H,22} = 0.14_{-0.10}^{+0.24}$, $kT_1 = 0.84_{-0.25}^{+0.18}$ keV, $EM_1 = 1.3_{-0.4}^{+0.4} \times 10^{56} \text{ cm}^{-3}$ and $EM_2/EM_1 \leq 0.55$ for $kT_2 = 3.45$ keV.

The value of EM_1 lies between 3 and 7 orders of magnitude above the typical values ($EM_1 = 0.1 - 3 \times 10^{53} \text{ cm}^{-3}$), for the fits performed with the maximum and minimum kT_2 respectively, assuming 2MASS 17141152–2931594 lies in NGC 6304. Thus, an object with a typical EM_1 would have to be at a distance less than ~ 330 pc.

The ratio of the two emission measures EM_2/EM_1 , however, is a distance independent value, that is in all cases ≥ 1 for coronally active stars (Dempsey et al. 1993). In both cases, the derived 90 per cent confidence upper limits given before lie below values observed from coronally active systems. Therefore, the observed X-ray spectrum is inconsistent with the typical two-temperature plasma of a coronally active star, independently of the distance of the IR counterpart.

In conclusion, the optical/IR colors and proper motion of the counterpart are in marginal agreement with those of a main sequence object located in the foreground of NGC 6304. However, the X-ray spectrum of XMMU 171411–293159 is inconsistent with those of typical coronally active stars. This was shown using a distance independent value. In addition, the possible optical variability of the star (in the B -band, see Sec. 3.2.2) presents further support that the star is not

merely a typical dwarf main sequence star. At the same time, the X-ray spectrum is consistent with a H atmosphere qLMXB at the distance of NGC 6304; and the V vs. B-V and J vs. J-K CMDs support interpretation of the 2MASS counterpart as a post-AGB star in NGC 6304, which is evolutionarily consistent with the X-ray spectrum of a qLMXB. Without excluding classification as a foreground star, we identify XMMU 171411–293159 as a candidate qLMXB in NGC 6304; however, an optical/IR spectrum of the 2MASS counterpart should be obtained to confirm that the IR source is an actual post-AGB star in NGC 6304, and not a marginally spectrally unusual, optically variable main-sequence star ($0.7\text{--}0.9 M_{\odot}$) at a distance of \sim few 100 pc.

3.3. XMMU 171421–292917 - Source #5

The NS H-atmosphere tabulated model applies for this low signal-to-noise source. The fit is statistically acceptable (χ_{ν}^2/dof (prob.) = 1.09/16 (0.36)) and the parameters are consistent with expected values ($kT_{\text{eff}} = 70_{-20}^{+28}$ eV and $R_{\infty} = 23_{-10}^{+69}$ km with $N_{H,22} = 0.266$; See Fig 9). When leaving N_H free, the fit results become χ_{ν}^2/dof (prob.) = 1.12/15 (0.33) with $N_{H,22} = 0.46_{-0.68}^{+0.42}$, $kT_{\text{eff}} = 49_{-32}^{+77}$ eV and $R_{\infty} \geq 8.9$ km (the upper bound error estimate failed to converge), i.e. consistent with the previous fit when N_H was fixed.

The `nsaggrav` model is then used to confirm the first fit with the NS H-atmosphere model. Even though acceptable (χ_{ν}^2/dof (prob.) = 1.23/16 (0.23)), the fit of this low signal-to-noise spectrum does not allow for representative error estimates, as explained in §2.3. The other two XSPEC neutron star atmosphere models also have the same issue. Also, the simultaneous fitting of the pn, MOS1 and MOS2 spectra did not provide an improvement of the uncertainties.

Using the online 2MASS-PSC catalogue, a possible counterpart, 2MASS 17142095–2929163 ($m_J = 13.063(29)$, $m_H = 12.645(33)$ and $m_K = 12.510(35)$), is identified at an angular distance of 0.45 arcsec. Using the same calculations as for source #9, the probability of finding a counterpart as bright or brighter, as close or closer is 0.084 per cent when 179 stars with magnitude $m_J \leq 13.063$ are found in an annulus of inner radius 2 arcmin and outer radius 4 arcmin around the optical centre of NGC 6304⁷, implying an association with 99.916 per cent confidence.

Using the procedure described in § 3.2.2, the bolometric magnitude and luminosity of the IR counterpart are calculated from the V-band magnitude $V = 14.85(5)$, the B-band magnitude $B = 14.75(9)$ and the color $B - V = 0.90(7)$ (S. Ortolani, private communication, 2008). The values found are $m_{\text{bol}} = m_K - A_K + BC_K = 12.82$, implying an absolute bolometric magnitude $M_{\text{bol}} = -1.07$. Therefore, the bolometric luminosity is $L_{\text{bol}} = 7.96 \times 10^{35}$ erg s⁻¹, when the bolometric luminosity for the zero absolute bolometric magnitude is 2.97×10^{35} erg s⁻¹. As a check on the value

⁷Prior to the astrometric correction using XMMU 171411–293159 and 2MASS 17141152–2931594, the angular distance between the X-ray and 2MASS sources was 1.59 arcsec. The corresponding association confidence would have been, in that case, 98.95 per cent.

calculated for the bolometric luminosity, a blackbody curve is fitted to the unabsorbed photometry in *BVJHK* bands, assuming the source at the distance of NGC 6304. This resulted in a best fit ($\chi^2/\text{dof} = 3.98$, for 3 dof) of $R = 5.87 \pm 0.14 R_\odot$, $T_{\text{eff}} = 7180 \pm 150 \text{ K}$, for a total luminosity of $L = 4\pi R^2 \sigma T_{\text{eff}}^4 = 3.15 \times 10^{35} \text{ erg s}^{-1}$; this is a factor $\times 2.5$ below that calculated using the *BC_K* calculation above.

If the X-ray emission is coming from the star 2MASS 17142095–2929163, the X-ray to optical flux ratio for this giant star is therefore $F_X/F_{\text{bol}} = 10^{-4.05}$. From the ROSAT All Sky Survey catalogue of bright late-type giant and supergiant (Hunsch et al. 1998), the mean calculated X-ray to optical flux ratio for all 450 stars observed in that catalogue is $F_X/F_{\text{bol}} = 10^{-5.6 \pm 0.6} (1\sigma)$. The 0.1–2.4 keV range was used to estimate the X-ray flux. The 2MASS counterpart and the X-ray source #5 are consistent with being a giant star (2.6σ). However, if X-rays from XMMU 171421–292917 were due to a typical giant star, then similar X-ray flux from other giant stars in this GC would be expected; yet no other giant star on the outskirts of this GC exhibit similar X-ray fluxes. Also, using the same comparison as in Sec 3.2.2, the X-ray to bolometric flux ratio, $F_X/F_{\text{bol}} = 9 \times 10^{-5}$ is consistent with a main-sequence foreground star, for which the X-ray to bolometric flux ratio saturates at 10^{-3} (Vilhu & Walter 1987).

An analysis similar to the one performed for XMMU 171411–293159 (§ 3.2) excludes the possibility that the system is coronally active. The results of the spectral fits with a 2-temperature Raymond-smith (RS) plasma are as follows. For $kT_2 = 0.93 \text{ keV}$ (χ_ν^2/dof (prob.) = 1.25/14 (0.23)), $N_{H,22} = 1.15_{-0.36}^{+1.27}$, $kT_1 = 0.11_{-0.06}^{+0.22} \text{ keV}$, $\text{EM}_1 = 2.4_{-2.1}^{+12.9} \times 10^{59} \text{ cm}^{-3}$ and $\text{EM}_2 \leq 3.9 \times 10^{55} \text{ cm}^{-3}$. In the case of $kT_2 = 3.45 \text{ keV}$ (χ_ν^2/dof (prob.) = 1.25/14 (0.23)), $N_{H,22} = 1.12_{-0.53}^{+1.12}$, $kT_1 = 0.11_{-0.06}^{+0.19} \text{ keV}$, $\text{EM}_1 = 2.1_{-1.5}^{+18.5} \times 10^{59} \text{ cm}^{-3}$ and $\text{EM}_2 \leq 5.5 \times 10^{54} \text{ cm}^{-3}$. Therefore, the distance independent value EM_2/EM_1 is $\lesssim 10^{-3}$ in both cases and lower than the value $\text{EM}_2/\text{EM}_1 \geq 1$ observed for known coronally active stars (Dempsey et al. 1993). Thus, the X-ray spectrum of this source is inconsistent with that of typical coronally active stars. In addition, the best fit galactic absorption N_H values, $N_{H,22} = 1.15_{-0.36}^{+1.27}$ or $N_{H,22} = 1.12_{-0.53}^{+1.12}$, for the two cases of the two-temperature RS plasma, are significantly larger than the value in the direction of NGC 6304 ($N_{H,22} = 0.266$). Therefore, assuming an uniform distribution of absorbing material, the best fit value of N_H provides further support that XMMU 171421–292917 is unlikely to be a coronally active star in the foreground of the GC.

We therefore conclude that that XMMU 171421–292917 is not a coronally active foreground star. Finally, since the X-ray source is spectrally consistent with a qLMXB at a distance of 6 kpc, we identify the X-ray source as a candidate qLMXB in NGC 6304 with an identified IR companion in NGC 6304.

To estimate the accretion rate, the series of relations in Verbunt & van den Heuvel (1995) (X-Ray binaries, section 11.3.3) are used. From the radius of the companion star ($R_2 = 9.7 R_\odot$), calculated with the temperature $T_{\text{eff}} = 6915 \text{ K}$ (which is worked out from Masana et al. (2006)) and the luminosity $L_{\text{bol}} = 7.96 \times 10^{35} \text{ erg s}^{-1}$, the companion core mass: $M_c = 0.27 M_\odot$ ($Z = 0.02$)

and $M_c = 0.31 M_\odot$ ($Z = 0.0001$) are estimated, where $y \equiv \ln(M_c/0.25 M_\odot)$ with $\ln(R_2/R_\odot)$ and $\ln(L_2/L_\odot)$ being third order polynomials of y where the polynomial coefficients are theoretical fits given in Verbunt & van den Heuvel (1995). From M_c and $\dot{M}_c = 1.37 \times 10^{-11} (L/L_\odot) M_\odot \text{yr}^{-1}$, \dot{R}_2/R_2 is estimated giving the evolution time-scale of the companion: $\tau \approx 2 \times 10^7 \text{yr}$ ($Z = 0.02$) and $\tau \approx 2.3 \times 10^7 \text{yr}$ ($Z = 0.0001$). Finally, the following relation:

$$\frac{\dot{R}_2}{R_2} = -2 \frac{\dot{M}_2}{M_2} \left(\frac{5}{6} - \frac{M_2}{M_1} \right) \quad (3)$$

is used to calculate the accretion rate \dot{M}_2 from the companion on to the neutron star, assuming $M_2 = 0.8 M_\odot$. We found that $\dot{M}_2 = -4.4 \times 10^{-9} M_\odot \text{yr}^{-1}$ ($Z = 0.02$) and $\dot{M}_2 = -3.8 \times 10^{-9} M_\odot \text{yr}^{-1}$ ($Z = 0.0001$). With this value of \dot{M}_2 (for $Z = 0.02$), the quiescent luminosity in the DCH model is estimated using models that include core neutrino emission (Yakovlev et al. 2003). The thermal X-ray luminosity, $L_{\text{thermal}} = 1.1 \times 10^{33} \text{erg s}^{-1}$, is roughly consistent with thermal emission from other transients with high time-average mass transfer rates (Heinke et al. 2007).

4. Discussion

4.1. Comparison with *ROSAT* Observations

NGC 6304 was observed once previously, using *ROSAT*/HRI (Rappaport et al. 1994, R94 hereafter), in which four X-ray sources were discovered. Three are spatially coincident with three X-ray sources detected in the present observations (in fact, the three correspond to the candidate qLMXBs). The fourth X-ray source in R94, however, appears to have faded significantly; the present observation detects no X-ray source consistent in position with *ROSAT* source D. The following analysis compares the position and fluxes of the for *ROSAT*/HRI sources.

The positions of the four sources in R94 have been examined and compared to those of X-ray sources in the present work. No positional uncertainties are given from analysis of R94. Using the archived *ROSAT*/HRI data at *HEASARC*, the positional uncertainties required for the comparison with the present *XMM-Newton* data were obtained. The source positions are consistent between the two different observations: source A, B and C in R94 corresponding to sources #4, #5 and #9 in this work. The boresight systematic uncertainty (6 arcsec) have been taken into account. For source D, no corresponding source is detected within 1 arcmin of the position for source D given by R94. A total of 304 counts are found in a 25 arcsec area around the position given by R94, while an average of 294.8 ± 2.2 are due to background using a nearby off-source area. This leaves 9 ± 18 counts due to a possible X-ray source at this position, consistent with no source detection.

There is a 3σ upper limit on the flux from source D of $F_X \leq 2.4 \times 10^{-14} \text{erg cm}^{-2} \text{s}^{-1}$ (0.5–2.4 keV), assuming a thermal bremsstrahlung spectrum with a temperature $kT = 3 \text{keV}$ (R94). By inspection of the MOS2 data, there is no evidence of any X-ray source in the vicinity of the position of source D.

Table 5 compares the predicted number of source counts which should be detected with *ROSAT*/HRI during the 5030 sec observation of R94, assuming the observed XMM/pn-med countrates and the XMM/pn source spectra, including both countrate and spectral uncertainties. For sources #4, #5, and #9, the expected number of counts (20.7 ± 1.5 , 3.9 ± 0.9 , 11.4 ± 1.0 , respectively) are consistent, within Poisson uncertainties, with the number of source counts observed by R94 (15, 7, and 17 respectively).

For source D, which is not detected, the 3σ upper limit on the number of counts due to an X-ray source at this position (<63 counts, in 11037 sec of integration), implies that <1.8 counts should have been detected with *ROSAT*/HRI, whereas the observed number of counts with *ROSAT*/HRI corresponds to 14 counts at the HRI field centre⁸. In an absence of an error analysis on the number of detected source counts from R94, it is not possible to correctly estimate the amount of fading; however, taking the detected number of counts at face value implies that source D faded in luminosity by a factor of ~ 10 .

In conclusion, the three qLMXBs are consistent with having the same luminosity between the *ROSAT*/HRI observation and the XMM/pn observation; and source D appears to have faded by a factor of ~ 10 .

4.2. Expected number of quiescent Neutron Stars in Globular Clusters

The number of X-ray binaries in a GC can be predicted from its internal properties. The encounter rate for a GC is predicted by $\Gamma \propto \rho_0^2/v$ where ρ_0 is the central luminosity density and v is the velocity dispersion (Verbunt 2002). For a virialized cluster, this relation simplifies to $\Gamma \propto \rho_0^{1.5} r_c^2$ where r_c is the core radius (in physical units, not angular distance). The number of quiescent NSs found in NGC 6304 is compared to the expected number of such objects from previous works (Gendre et al. 2003a; Heinke et al. 2003c).

In the first one (Table 2 and Figure 3 in Gendre et al. (2003a)), the authors found a linear relation between the number of quiescent NSs and the encounter rate: $N_{qNS} \sim 0.04 \times \Gamma + 0.2$. Using the same normalisation ($\Gamma_{\text{NGC 6440}} = 100$), the encounter rate of NGC 6304 is $\Gamma_{\text{NGC 6304}} = 6.4$. The predicted number of qLMXBs is therefore about 0.46. Assuming that three qLMXBs were found, this number seems slightly in excess of the prediction but the probability of finding such objects when the average expected number is 0.46 is 3.2 per cent, assuming Poisson statistics. This probability is not small enough to affirm that there is an inconsistency between the expected and the actual number.

⁸The number of counts given by R94 are corrected for scattering and vignetting by a factor >1 , but which is not given by R94. Therefore while R94 gives the number of counts which would have been detected from this source if it had been located at the centre of the FOV, the number of counts detected was not noted, and so the uncertainty in the number of counts has not been determined.

The second paper (Table 1 in Heinke et al. (2003c)) compared the encounter rate (normalised to the galactic value) to the number of accreting NS systems. The linear relation obtained from the data collected in this previous work is simply $N = 0.993 \times \Gamma - 0.046$, for which the expected number of accreting NSs in NGC 6304 is 0.38. Again, three qLMXBs is a number that seems larger than the expectation, but certainly not inconsistent.

Finally, the encounter rate can be compared to the number of X-ray sources in the GC (Pooley et al. 2003). The expected number of X-ray sources for an encounter rate $\Gamma_{NGC\ 6304} = 45$ is about 9.5, comparable with the seventeen sources detected in the FOV. The following subsection discuss the number of background sources that are expected to be detected in the field of view of the observation.

4.3. Background X-ray sources expected in the field of NGC 6304

To estimate the number of expected Active Galactic Nuclei (AGN) detected during the observation of NGC 6304, the field of the pn camera is divided into 3 concentric annuli centred at the centre of the exposure map (with radii between 0 and 5, 5 and 10, and between 10 and 13 arcmin). The limiting flux in each annulus is estimated using the lowest count rate detected (4.3 counts per sec) and the tool *webPIMMS*, to obtain the absorbed flux a power-law of photon index 2. The limiting fluxes are 1.8×10^{-14} erg cm⁻² s⁻¹, 1.2×10^{-14} erg cm⁻² s⁻¹, and 0.9×10^{-14} erg cm⁻² s⁻¹, for the three annuli respectively. Using the number-flux (LogN-LogS) distribution function for X-ray AGN (Hasinger 1993, H93 hereafter), the number of expected background X-ray sources is 0.87 ± 0.1 , 5.22 ± 0.28 and 10.7 ± 0.75 in the three annuli, respectively, corresponding to a total of 17 ± 1 over the whole field. This result is consistent with the number of sources detected in the field, and with the tentative conclusion claiming that 3 qLMXBs are detected in the GC NGC 6304. However, the error bars only takes into account the uncertainty in the LogN-LogS relation and not in the limiting fluxes and are therefore likely to be underestimated.

5. Summary and Conclusions

The globular cluster NGC 6304 hosts three candidate qLMXBs. The neutron star radii and temperatures obtained for the three candidates are consistent with typical values for neutron stars and in accordance with radii of other known field and GCs qLMXBs. No variability is measured from any of the candidates over the time scale of the observation, with very weak limits; the large X-ray variability in the *XMM-Newton*/pn background precludes a more detailed variability analysis. A comparison with *ROSAT* observations 14 yr prior (R94), finds the fluxes of the candidates are consistent with those of the earlier observation (R94). The absence of a detailed error analysis in the fluxes from the published *ROSAT* analysis precludes placing statistical limit on the amount of variability; however, as the number of detected counts in the *ROSAT* observations was small

(<20), the magnitude of intensity variability is limited to be less than a factor of \sim few on the 14-yr time-scale.

XMMU 171433–292747 is located in the core ($0.79 r_c$) of the GC. Its spectrum is acceptably fitted with a NS Hydrogen atmosphere model with $kT_{\text{eff}} = 122^{+31}_{-45}$ eV and $R_\infty = 11.6^{+6.3}_{-4.6}$ km, combined with a power-law component of photon index $\alpha = 1.2^{+0.7}_{-0.8}$. The power-law component dominates the spectrum at photon energies above 2 keV, and represents 49 per cent of the observed flux (0.5–10 keV). This contribution, although its source is not perfectly understood, is similar to that found in some other qLMXBs, and is comparable in the fraction of the flux for which it accounts to the field qLMXB Cen X-4 (Asai et al. 1996b; Rutledge et al. 2001b; Menou & McClintock 2001; Campana et al. 2004). While the high stellar density in the core of NGC 6304 precludes identification of a 2MASS counterpart for XMMU 171433–292747, a visual overlap with a 2MASS image of the GC shows a possible association with an uncatalogued – and likely unresolved – star. The association will require further investigation with higher resolution optical/IR imaging.

XMMU 171421–292917, a second candidate, has a low signal-to-noise and correspondingly larger error bars for the X-ray spectral parameters used to identify it as a qLMXB candidate: the NS H-atmosphere temperature is 70^{+28}_{-20} eV, and $R_\infty = 23^{+69}_{-10}$ km. A faint 2MASS counterpart ($m_J = 13.063$) is identified (with 99.916 per cent confidence), and the X-ray emission is unlikely to emerge from the giant star itself.

XMMU 171411–293159, a third candidate, is a bright X-ray source consistent with a neutron star H atmosphere spectral model at the distance of the GC. Its measured properties are $kT_{\text{eff}} = 115^{+21}_{-16}$ eV and $R_\infty = 10.7^{+6.3}_{-3.1}$ km. The 2MASS IR counterpart (with 99.988 per cent confidence) appears to belong to the post-asymptotic giant branch; this is the first qLMXB with this type of companion. Other explanations for the source are investigated, concluding that a coronally active field star is not a possible explanation, due to the unusual optical/IR colors and unusual X-ray spectrum. Optical/IR spectroscopy of 2MASS 17141152–2931594 can definitively determine whether the star is a foreground main sequence star, or an evolved post-AGB star at the distance of NGC 6304.

A faint unidentified X-ray source showing an unusual excess of high energy photons resulting in a photon index of $\alpha = -2.0^{+1.2}_{-2.2}$. The nature of this source is unclear. There is no evidence the X-ray source was variable during the observation. No off-band counterparts in the 2MASS or DSS catalogues are found within 3σ of the X-ray position. Deep observations in the off-bands, as well as repeated detection and study in the X-ray, can inform interpretation of this source.

The qLMXB candidates in NGC 6304 are astronomically interesting. First, the number of candidates is consistent with predictions from the calculated encounter rate, supporting previous observational analyses which characterised the qLMXB rate vs. encounter rate in GCs (Pooley et al. 2003; Heinke et al. 2003c; Gendre et al. 2003a). This indicates that the qLMXB rate vs. encounter rate is not merely a parameterisation resulting from observations, but can predict the number of qLMXBs in unobserved GCs.

NGC 6304 contains one of the most luminous known qLMXBs. XMMU 171433–292747, with a intrinsic luminosity $L_X = 10^{33}$ erg s⁻¹ (0.5–10 keV), is the fourth most luminous GC qLMXB after 47 Tuc X7 ($L_X = 1.5 \times 10^{33}$ erg s⁻¹ (0.5–10 keV)), 47 Tuc X5 ($L_X = 1.4 \times 10^{33}$ erg s⁻¹ (0.5–2.5 keV)) and the qLMXB in M28 ($L_X = 1.2 \times 10^{33}$ erg s⁻¹ (0.5–10 keV)). These represent the upper limit of the expected luminosity for LMXB in quiescence. In addition, XMMU 171433–292747, with its high flux ($F_X = 2.3 \times 10^{-13}$ erg cm⁻² s⁻¹, after 47 Tuc X7, 47 Tuc X5 and the qLMXB in M28 with fluxes 5.3, 4.3 and $3.3_{-1.1}^{+1.9} \times 10^{-13}$ erg cm⁻² s⁻¹, respectively - see Table 4), is a good candidate to constrain the equation of state of dense matter.

NGC 6304 hosts two candidate qLMXBs lying at large distance from the hosting core, but still within the tidal radius; XMMU 171411–293159 and XMMU 171421–292917 are located at $\sim 32r_c$ and $\sim 15r_c$, respectively. Previously, all GC qLMXBs were located within $< 7r_c$ of the optical centre of their GC (see Table 6), the most distant belonging to U24 in NGC 6397, located $6.8r_c$ from the centre; noting, however, that NGC 6397 is a core collapse GC with $r_c = 0.05'$. To sum up, the qLMXB candidates in NGC 6304 are of much greater distance from the GC centre than has been observed previously, and may require revisiting theory of qLMXB formation and binary evolution in GC.

Deeper X-ray exposures are required to confirm the classification of the candidates qLMXB found in NGC 6304. Specifically, it is necessary to constrain R_∞ to an uncertainty of few percent (as already performed for confirmed qLMXBs in ω Cen and 47 Tuc, see Table 4) rather than few tens of percent here. For XMMU 171433–292747, better angular resolution will confirm the isolated nature of the candidate qLMXB, or may resolve multiple X-ray sources in the core. New deep observations of XMMU 171421–292917 and XMMU 171411–293159 will produce a localisation unbiased by bad detector columns. At optical wavelengths, observations of the aforementioned candidates can determine unequivocally the evolutionary state of the counterparts (a giant for 2MASS 17142095–2929163, and a post-AGB star for 2MASS 17141152–2931594), as well as measure their binary orbital periods through ellipsoidal variations. The spatial isolation and brightness of the IR counterparts implies this work can be done easily using ground based, moderate sized telescopes. Optical spectroscopic observations can confirm that the counterparts have radial velocities consistent with that of NGC 6304. Finally, high spatial resolution observations of the GC core in the optical/IR bands can pinpoint a possible counterpart for XMMU 171433–292747 and confirm the qLMXB nature of this X-ray source.

Robert E. Rutledge is supported by an NSERC Discovery grant. Edward F. Brown and Vyacheslav E. Zavlin acknowledge support from NASA under award No. NNX06AH79G. The authors are particularly thankful to Prof. Sergio Ortolani for providing the V-band magnitude data of stars in the GC, especially for the two aforementioned counterparts, to calculate the bolometric luminosities and produce the V vs $(B - V)$ diagram. Finally, the authors would like to thank the referee for fruitful remarks.

REFERENCES

- Arnaud, K. A. 1996, in *Astronomical Data Analysis Software and Systems V.*, ed. G. Jacoby & J. Barnes, Vol. 101 (ASP Conf. Series), 17
- Asai, K., Dotani, T., Hoshi, R., Tanaka, Y., Robinson, C. R., & Terada, K. 1998, *PASJ*, 50, 611
- Asai, K., Dotani, T., Mitsuda, K., Hoshi, R., Vaughan, B., Tanaka, Y., & Inoue, H. 1996b, *PASJ*, 48, 257
- Becker, W. et al. 2003, *ApJ*, 594, 798
- Bildsten, L. & Chakrabarty, D. 2001, *ApJ*, 557, 292
- Bildsten, L., Salpeter, E. E., & Wasserman, I. 1992, *ApJ*, 384, 143
- Bloecker, T. 1995, *A&A*, 299, 755
- Brown, E. F., Bildsten, L., & Rutledge, R. E. 1998, *ApJ*, 504, L95
- Cackett, E. M., Wijnands, R., Linares, M., Miller, J. M., Homan, J., & Lewin, W. H. G. 2006, *MNRAS*, 372, 479
- Campana, S., Israel, G. L., Stella, L., Gastaldello, F., & Mereghetti, S. 2004, *ApJ*, 601, 474
- Campana, S. & Stella, L. 2000, *ApJ*, 541, 849
- Campana, S., Stella, L., Mereghetti, S., & Cremonesi, D. 2000, *A&A*, 358, 583
- Caputo, F. 1985, *Reports of Progress in Physics*, 48, 1235
- Clark, G. W. 1975, *ApJ*, 199, L143
- Cornelisse, R., Wijnands, R., & Homan, J. 2007, *MNRAS*, 380, 1637
- de Bruijne, J. H. J., Hoogerwerf, R., & de Zeeuw, P. T. 2001, *A&A*, 367, 111
- Dempsey, R. C., Linsky, J. L., Schmitt, J. H. M. M., & Fleming, T. A. 1993, *ApJ*, 413, 333
- Dickey, J. M. & Lockman, F. J. 1990, *ARA&A*, 28, 215
- Edmonds, P. D., Heinke, C. O., Grindlay, J. E., & Gilliland, R. L. 2002, *ApJ*, 564, L17
- Fitzpatrick, E. L. 1999, *PASP*, 111, 63
- Fruscione, A. et al. 2006, in *Observatory Operations: Strategies, Processes, and Systems.*, Vol. 6270, Ed. Silva, D. R.; Doxsey, R. E. *Proceedings of the SPIE Conf.*
- Garcia, M. R. 1994, *ApJ*, 435, 407

- Gendre, B., Barret, D., & Webb, N. 2003a, *A&A*, 403, L11
- Gendre, B., Barret, D., & Webb, N. A. 2003b, *A&A*, 400, 521
- Gnedin, O. Y., Zhao, H., Pringle, J. E., Fall, S. M., Livio, M., & Meylan, G. 2002, *ApJ*, 568, L23
- Grindlay, J. E., Heinke, C., Edmonds, P. D., & Murray, S. S. 2001a, *Science*, 292, 2290
- Grindlay, J. E., Heinke, C. O., Edmonds, P. D., Murray, S. S., & Cool, A. M. 2001b, *ApJ*, 563, L53
- Guainizzi, M. 2008, XMM Newton Science Operation Centre, Calibration Report XMM-SOC-CAL-TN-0018, available at http://xmm.vilspa.esa.es/external/xmm_sw_cal/calib/documentation/index.shtml
- Gupta, S., Brown, E. F., Schatz, H., Möller, P., & Kratz, K. 2007, *ApJ*, 662, 1188
- Haensel, P. & Zdunik, J. L. 1990, *A&A*, 227, 431
- 2003, *A&A*, 404, L33
- 2008, *A&A*, 480, 459
- Haggard, D., Cool, A. M., Anderson, J., Edmonds, P. D., Callanan, P. J., Heinke, C. O., Grindlay, J. E., & Bailyn, C. D. 2004, *ApJ*, 613, 512
- Harris, W. E. 1996, *AJ*, 112, 1487
- Harwit, M. 2006, *Astrophysical Concepts (Astrophysical Concepts, by Martin Harwit. ISBN 978-0-387-32943-7. Berlin: Springer, 2006.)*
- Hasinger, G. 1993, *Advances in Space Research*, 13, 241
- Heinke, C. O., Grindlay, J. E., & Edmonds, P. D. 2005, *ApJ*, 622, 556
- Heinke, C. O., Grindlay, J. E., Edmonds, P. D., Lloyd, D. A., Murray, S. S., Cohn, H. N., & Lugger, P. M. 2003a, *ApJ*, 598, 516
- Heinke, C. O., Grindlay, J. E., Lloyd, D. A., & Edmonds, P. D. 2003b, *ApJ*, 588, 452
- Heinke, C. O., Grindlay, J. E., Lugger, P. M., Cohn, H. N., Edmonds, P. D., Lloyd, D. A., & Cool, A. M. 2003c, *ApJ*, 598, 501
- Heinke, C. O., Jonker, P. G., Wijnands, R., & Taam, R. E. 2007, *ApJ*, 660, 1424
- Heinke, C. O., Rybicki, G. B., Narayan, R., & Grindlay, J. E. 2006, *ApJ*, 644, 1090
- Hunsch, M., Schmitt, J. H. M. M., & Voges, W. 1998, *A&AS*, 127, 251

- Hut, P. et al. 1992, *PASP*, 104, 981
- in't Zand, J. J. M., van Kerkwijk, M. H., Pooley, D., Verbunt, F., Wijnands, R., & Lewin, W. H. G. 2001, *ApJ*, 563, L41
- Ivanova, N. 2006, *ApJ*, 636, 979
- Jacoby, G. H., Morse, J. A., Fullton, L. K., Kwitter, K. B., & Henry, R. B. C. 1997, *AJ*, 114, 2611
- Jeffries, R. D., Evans, P. A., Pye, J. P., & Briggs, K. R. 2006, *MNRAS*, 367, 781
- Jonker, P. G., Bassa, C. G., & Wachter, S. 2007a, *MNRAS*, 377, 1295
- Jonker, P. G., Steeghs, D., Chakrabarty, D., & Juett, A. M. 2007b, *ApJ*, 665, L147
- Kundu, A., Maccarone, T. J., & Zepf, S. E. 2002, *ApJ*, 574, L5
- Lattimer, J. M. & Prakash, M. 2004, *Science*, 304, 536
- Lugger, P. M., Cohn, H. N., Heinke, C. O., Grindlay, J. E., & Edmonds, P. D. 2007, *ApJ*, 657, 286
- Maccarone, T. J., Kundu, A., & Zepf, S. E. 2003, *ApJ*, 586, 814
- Marigo, P., Girardi, L., Bressan, A., Groenewegen, M. A. T., Silva, L., & Granato, G. L. 2008, *A&A*, 482, 883
- Masana, E., Jordi, C., & Ribas, I. 2006, *A&A*, 450, 735
- McClintock, J. E., Narayan, R., & Rybicki, G. B. 2004, *ApJ*, 615, 402
- Menou, K. & McClintock, J. E. 2001, *ApJ*, 557, 304
- Monet, D. G. et al. 2003, *AJ*, 125, 984
- Montalbán, J., Miglio, A., Noels, A., Grevesse, N., & di Mauro, M. P. 2004, in *ESA Special Publication*, Vol. 559, *SOHO 14 Helio- and Asteroseismology: Towards a Golden Future*, ed. D. Danesy, 574–+
- Ortolani, S., Momany, Y., Bica, E., & Barbuy, B. 2000, *A&A*, 357, 495
- Pooley, D. et al. 2003, *ApJ*, 591, L131
- Rajagopal, M. & Romani, R. W. 1996, *ApJ*, 461, 327
- Rappaport, S., Dewey, D., Levine, A., & Macri, L. 1994, *ApJ*, 423, 633
- Rieke, G. H. & Lebofsky, M. J. 1985, *ApJ*, 288, 618
- Rutledge, R. E., Bildsten, L., Brown, E. F., Pavlov, G. G., & Zavlin, V. E. 1999, *ApJ*, 514, 945

- 2000, ApJ, 529, 985
- 2001a, ApJ, 559, 1054
- 2001b, ApJ, 551, 921
- 2002a, ApJ, 578, 405
- Rutledge, R. E., Bildsten, L., Brown, E. F., Pavlov, G. G., Zavlin, V. E., & Ushomirsky, G. 2002b, ApJ, 580, 413
- Schatz, H. et al. 2001, Physical Review Letters, 86, 3471
- Schatz, H., Bildsten, L., Cumming, A., & Wiescher, M. 1999, ApJ, 524, 1014
- Secker, J. 1992, AJ, 104, 1472
- Servillat, M., Webb, N. A., & Barret, D. 2008, A&A, 480, 397
- Singh, K., Drake, S., & White, N. 1996, AJ, 111, 2415
- Siódmiak, N., Meixner, M., Ueta, T., Sugerman, B. E. K., Van de Steene, G. C., & Szczerba, R. 2008, ApJ, 677, 382
- Sivakoff, G. R. et al. 2007, ApJ, 660, 1246
- Strüder, L. et al. 2001, A&A, 365, L18
- Tomsick, J. A., Gelino, D. M., Halpern, J. P., & Kaaret, P. 2004, ApJ, 610, 933
- Tomsick, J. A., Gelino, D. M., & Kaaret, P. 2005, ApJ, 635, 1233
- 2007, ApJ, 663, 461
- Ushomirsky, G. & Rutledge, R. E. 2001, MNRAS, 325, 1157
- Valenti, E., Ferraro, F. R., & Origlia, L. 2007, AJ, 133, 1287
- Valenti, E., Origlia, L., & Ferraro, F. R. 2005, MNRAS, 361, 272
- Van Paradijs, J., Verbunt, F., Shafer, R. A., & Arnaud, K. A. 1987, A&A, 182, 47
- Verbunt, F. 2002, in Astronomical Society of the Pacific Conference Series, Vol. 296, New Horizons in Globular Cluster Astronomy, ed. G. Piotto, G. Meylan, S. G. Djorgovski, & M. Riello, p 245
- Verbunt, F., Belloni, T., Johnston, H. M., van der Klis, M., & Lewin, W. H. G. 1994, A&A, 285, 903

- Verbunt, F. & van den Heuvel, E. P. J. 1995, in X-ray binaries, Ed. Lewin, W., van Paradijs, J., and van den Heuvel, E. P. J., Cambridge University Press, p 457–494
- Vilhu, O. & Walter, F. M. 1987, ApJ, 321, 958
- Webb, N. A., Wheatley, P. J., & Barret, D. 2006, A&A, 445, 155
- Wijnands, R., Heinke, C. O., & Grindlay, J. E. 2002, ApJ, 572, 1002
- Wijnands, R., Miller, J. M., Markwardt, C., Lewin, W. H. G., & van der Klis, M. 2001, ApJ, 560, L159
- Yakovlev, D. G., Gasques, L., & Wiescher, M. 2006, MNRAS, 371, 1322
- Yakovlev, D. G., Levenfish, K. P., & Haensel, P. 2003, A&A, 407, 265
- Zavlin, V. E., Pavlov, G. G., & Shibanov, Y. A. 1996, A&A, 315, 141

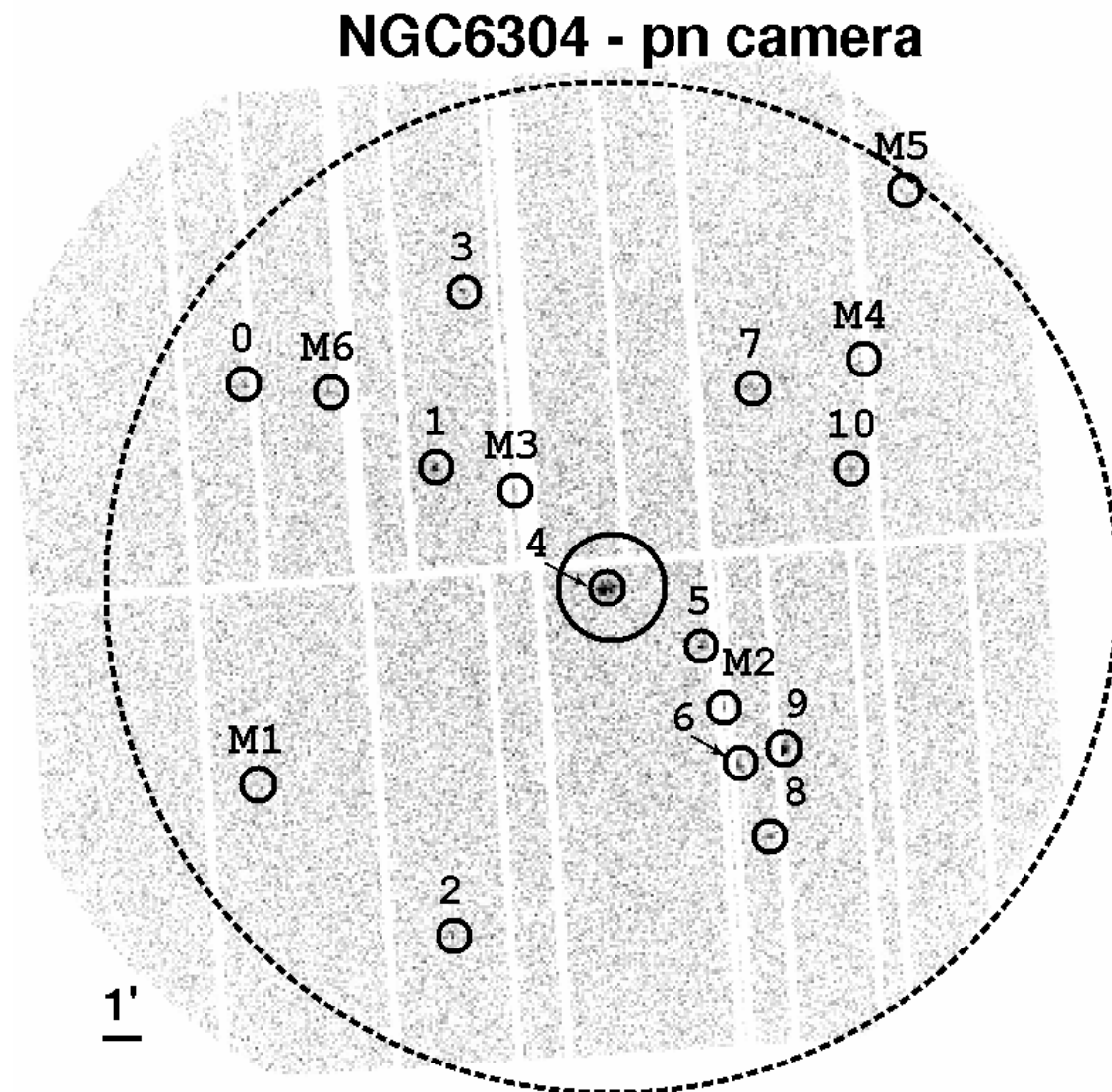


Fig. 1.— XMM/pn image of the globular cluster NGC 6304. Each small circle shows the position of the 17 detected sources. The small circles labelled M1 through M6 correspond to sources detected on the MOS cameras only. The bigger solid circle and large dashed circle represent the half mass radius and the tidal radius (respectively) of NGC 6304. The values $r_{\text{HM}} = 1.41'$ and $r_t = 13.25'$ are from the Harris catalogue of globular clusters (Harris 1996). The source numbers correspond to those in Table 1 and Table 2.

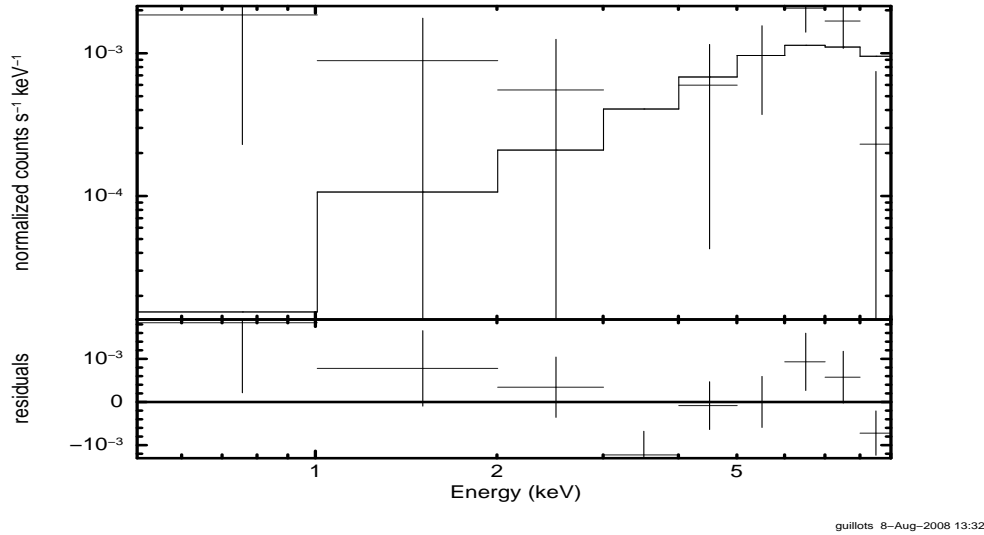


Fig. 2.— Folded spectrum of source #8 (XMMU 171413–293415) fitted with an absorbed power law model ($\alpha = -2.0_{-2.2}^{+1.2}$) with the H-absorption fixed $N_{H,22} = 0.266$. The binning of the counts is different from the standard binning (minimum of 20 or 25 counts per bin). Due to the low signal-to-noise of this source, bins of 1 keV width (except for the 0.5 to 1 keV bin) are chosen.

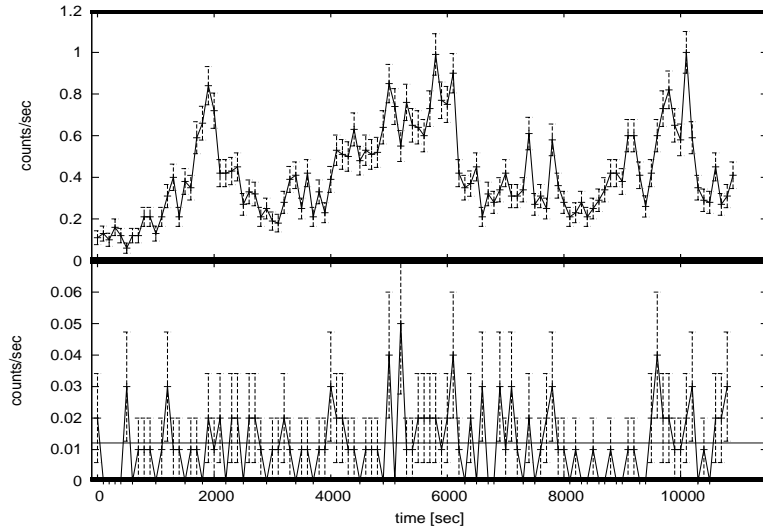


Fig. 3.— Lightcurve between 5 and 10 keV, with 100 sec bins. Bottom: lightcurve of extraction circular region of source #8 (25 arcsec). The horizontal line at 0.0121 counts/sec (0.0078 background counts/sec expected) is the mean count rate. Top: lightcurve of the background area chosen for source #8.

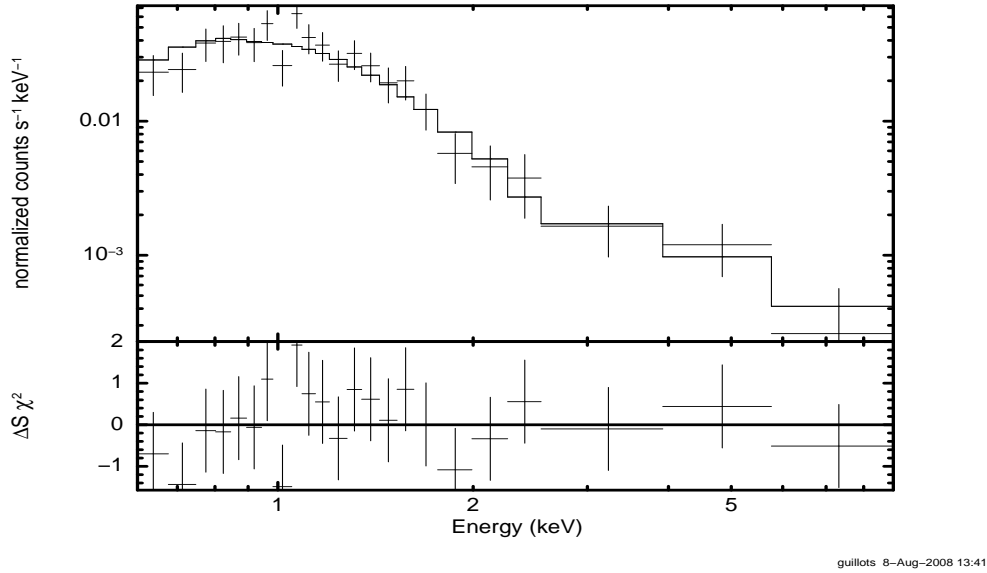


Fig. 4.— Folded model to the pn camera spectrum of source #4 (XMMU 171433–292747). The solid line is the best fit model of a neutron star atmosphere `nsa` ($N_{H,22} = 0.266$ held fixed) together with a power-law component of slope $\alpha = 1.2^{+0.7}_{-0.8}$. Due to the low signal-to-noise at large energies (above 2.5 keV), the last 9 bins are grouped into three separate bins.

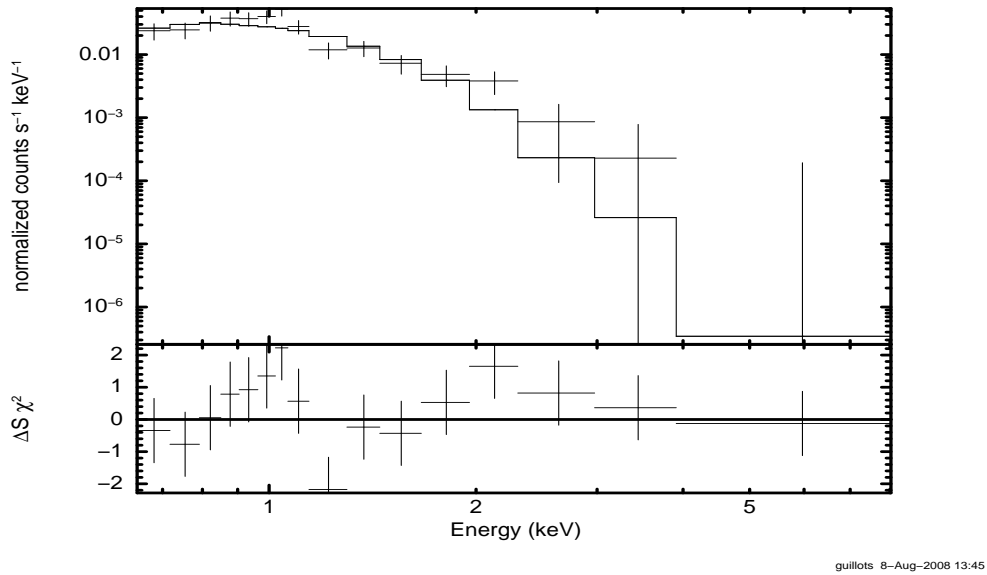


Fig. 5.— Folded model to the pn camera spectrum of source #9 (XMMU 171411–293159). The solid line is the best fit (tabulated) model of a NS H-atmosphere ($N_{H,22} = 0.266$ held fixed). Due to the low signal-to-noise at large energies, the last three bins are grouped into a single bin above 4 keV.

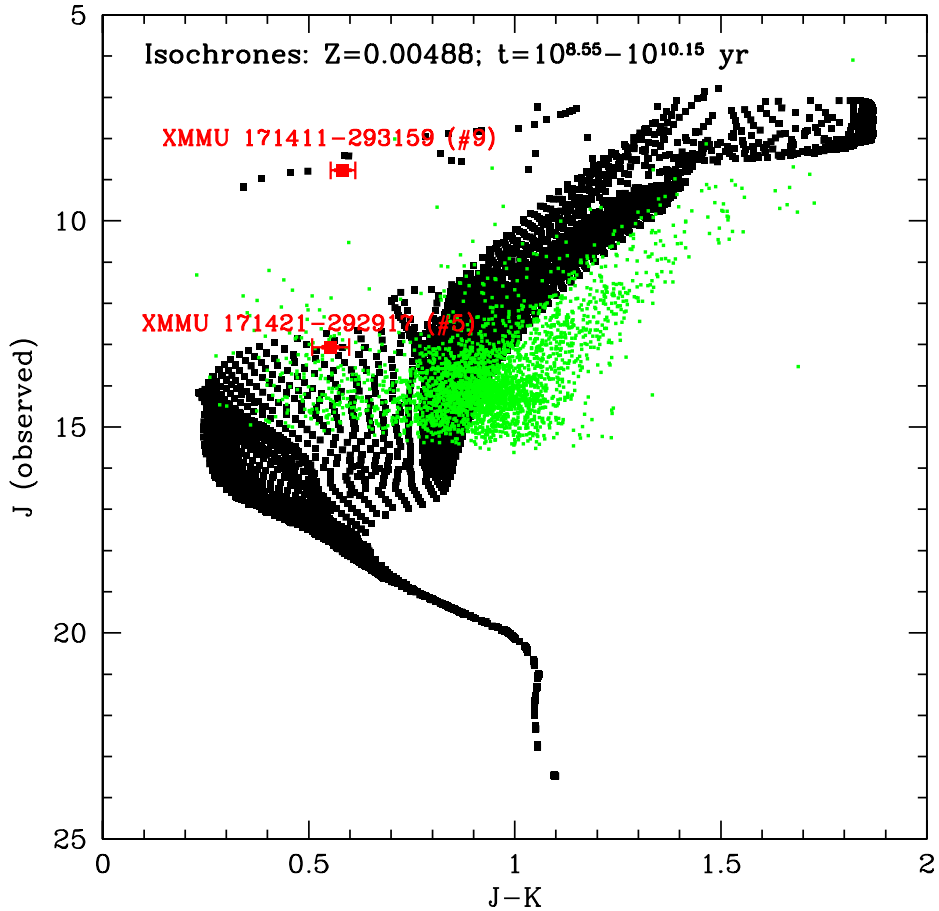


Fig. 6.— Color (J-K) Magnitude (K-band) diagram of the globular cluster NGC 6304 showing isochrones (small squares) for ages in the range $t = 10^{8.55} - 10^{10.15}$ yr and $Z = 0.00488$ (Marigo et al. 2008). All 2MASS catalogued stars (small dots) within 6.5 arcmin of the optical centre of the cluster are included, down to a magnitude of $m_K \sim 15$. The large squares with error bars are the IR counterparts to source #9 and #5, with $m_J = 8.769$ and $m_K = 13.063$, respectively. This diagram suggests that the counterpart for XMMU 171411–293159 belongs to the post-asymptotic giant branch. A spatial analysis of the stars that lie redward of the giant branch compared to those that lie blueward shows that there is an over-density of bluer stars near the GC core. In other words, redder stars are less likely to belong to the GC and are likely to be contaminating field stars. Thus, contamination by field stars can explain the poor matching between the theoretical isochrones and the actual data.

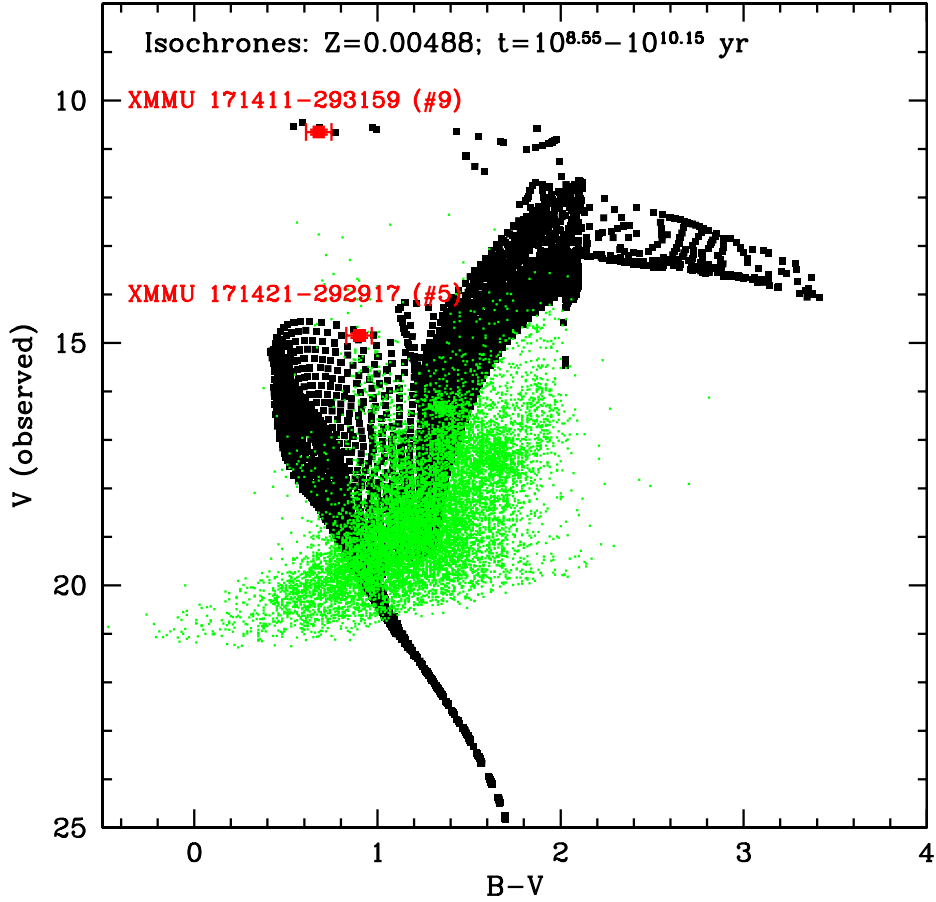


Fig. 7.— Color (B-V) Magnitude (V-band) diagram of the globular cluster NGC 6304 with the isochrones (small squares) for ages in the range $t = 10^{8.55} - 10^{10.15}$ yr and $Z = 0.00488$ (Marigo et al. 2008). Also included are all the stars (small dots) within 6.5 arcmin of the optical centre (S. Ortolani, private communication, 2008 and Ortolani et al. (2000)) down to a limiting magnitude of $V \sim 21$. The large squares with error bars are the optical counterparts to source #9 and #5, with $V = 10.65$ and $V = 14.85$, respectively. Similarly to Fig 6, this suggests that the counterpart for XMMU 171411–293159 is a post-AGB star at the distance of NGC 6304. Also, field contamination could be responsible for the poor matching between the theoretical isochrones and the actual 2MASS data.

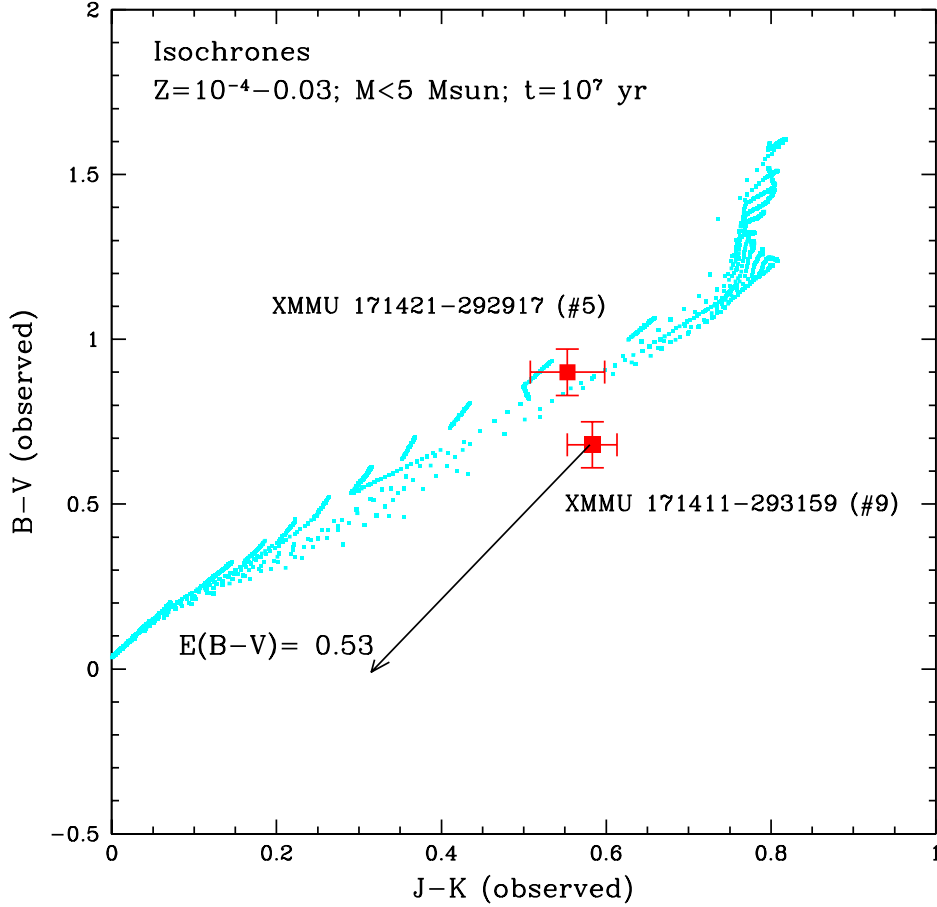


Fig. 8.— Color ($J - K$) Color ($B - V$) diagram showing isochrones of low-mass ($M < 5 M_{\odot}$) stars at $t = 10^7$ yr (small points) for a range of metallicities ($Z = 0.0001 - 0.03$, $\Delta Z = 0.0005$). The large points with error bars are corresponding to XMMU 171421-292917 (#5) and XMMU 171411-293159 (#9). In considering source #9 as a foreground coronally active star, it lies marginally off the main sequence (between $2-3\sigma$) at zero reddening ($E(B - V) = 0$). The discrepancy worsens if source #9 is at greater reddening; the vector beginning at source #9 terminates at the intrinsic color 2MASS 17141152-2931594 would be at $E(B - V) = 0.53$, that of NGC 6304. This does not support the hypothesis that XMMU 171411-293159 is a typical coronally active star, in the foreground of NGC 6304.

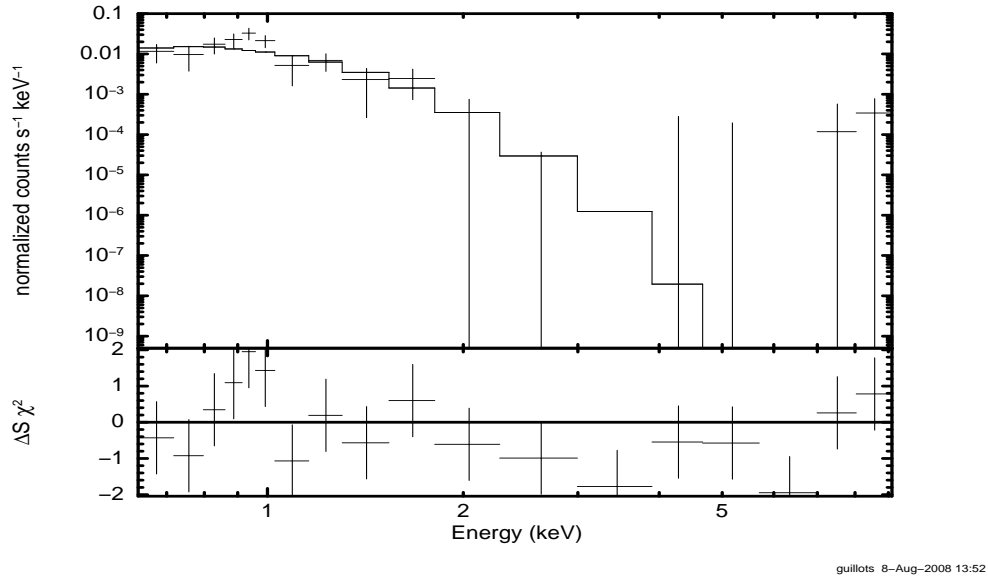


Fig. 9.— Folded model Spectrum of source #5 (XMMU 171421–292917). The solid line is the best fit (tabulated) model of a neutron star atmosphere ($N_{H,22} = 0.266$ held fixed).

Table 1. X-ray Catalogue of sources in the field of NGC 6304 (Astrometry)

Object Name	R.A. (J2000)	Decl. (J2000)	$\delta_{R.A.} \setminus \delta_{Decl.}^a$ (arcsec)	Δ/r_c^b	ID
XMMU 171403–292438	258.51323	-29.41030	$\pm 0.5 \setminus 0.5$	33.4	10
XMMU 171411–293159	258.54803	-29.53317	$\pm 0.5 \setminus 0.4$	31.8	9
XMMU 171413–293415	258.55432	-29.57151	$\pm 1.0 \setminus 0.8$	38.6	8
XMMU 171415–292232	258.56320	-29.37568	$\pm 0.9 \setminus 0.8$	31.9	7
XMMU 171417–293222	258.57100	-29.53968	$\pm 0.9 \setminus 1.0$	28.5	6
XMMU 171421–292917	258.58731	-29.48801	$\pm 0.8 \setminus 1.0$	15.2	5
XMMU 171433–292747	258.63636	-29.46310	$\pm 0.7 \setminus 0.6$	0.79	4
XMMU 171449–292001	258.70731	-29.33378	$\pm 1.0 \setminus 0.9$	42.3	3
XMMU 171451–293653	258.71296	-29.61490	$\pm 1.0 \setminus 0.9$	49.1	2
XMMU 171453–292436	258.72141	-29.41001	$\pm 0.7 \setminus 0.6$	29.2	1
XMMU 171516–292224	258.81800	-29.37320	$\pm 0.5 \setminus 0.5$	52.2	0

Note. — The sources are sorted by increasing R.A. Both coordinates (R.A. and Decl.) are given in decimal degrees, after the astrometric correction.

^aStatistical uncertainty from the source detection in seconds of arc.

^bdistance from GC centre in r_c units - $r_c=0.21'$ (Harris 96).

Table 2. X-ray Catalogue of sources in the field of NGC 6304 detected with the MOS camera only

Object Name	R.A. (J2000)	Decl. (J2000)	$\delta_{R.A.} \setminus \delta_{Decl.}^a$ (arcsec)	S/N	Rate (cts ks ⁻¹)	ID
XMMU 171514–293254	258.81098	-29.54841	$\pm 1.1 \setminus 0.8$	4.3	2.8±0.8	M1
XMMU 171418–293053	258.57689	-29.51474	$\pm 0.7 \setminus 0.8$	7.1	3.1±0.6	M2
XMMU 171443–292511	258.68223	-29.41987	$\pm 0.6 \setminus 0.6$	5.1	2.0±0.5	M3
XMMU 171401–292145	258.50750	-29.36265	$\pm 1.0 \setminus 0.6$	6.3	3.3±0.7	M4
XMMU 171356–291720	258.48705	-29.28889	$\pm 0.7 \setminus 1.0$	4.5	3.4±0.9	M5
XMMU 171505–292235	258.77451	-29.37666	$\pm 1.2 \setminus 0.7$	5.6	3.6±0.8	M6

Note. — The right ascension (R.A.) and declination (Decl.) are given in decimal degrees.

^aStatistical uncertainty from the source detection in seconds of arc.

Table 3. X-ray Catalogue of sources in the field of NGC 6304 (Fluxes)

ID	S/N	Rate ^a (cts ks ⁻¹)	kT_{eff} ^b (eV)	α ^b	χ^2_{ν}/dof (prob.)	F_X ^c	Type ^d
10	5.2	4.5±1.9	–	(1) *	0.74/16 (0.76)	0.37	??
9	20.2	25.2±2.2	115 ⁺²¹ ₋₁₆	–	1.20/31 (0.21)	1.52	qNS?
8	5.3	7.1±2.0	–	-2.0 ^{+1.2} _{-2.2}	1.73/7 (0.10)	2.8	??
7	4.3	4.3±1.9	–	(1) *	0.84/16 (0.63)	0.37	??
6	8.0	7.2±1.7	–	(1) *	0.75/13 (0.71)	0.76	??
5	7.0	9.1±2.0	70 ⁺²⁸ ₋₂₀	–	1.09/16 (0.36)	0.59	qNS?
4	19.3	43.8±2.8	122 ⁺³¹ ₋₄₅	1.2 ^{+0.7} _{-0.8}	0.85/42 (0.75)	2.3	qNS?
3	4.3	6.2±1.9	–	(1) *	0.68/16 (0.82)	0.77	??
2	5.4	6.1±1.9	–	(1) *	1.37/15 (0.15)	0.86	??
1	8.3	15.3±2.1	–	0.52±0.34	0.96/15 (0.50)	2.47	??
0	4.7	10.3±1.7	–	-0.3 ^{+0.7} _{-0.5}	0.84/12 (0.60)	4.2	??

Note. — N_H column density fixed to $N_{H,22} = 0.266$ for all spectral fits.

^aBackground subtracted count rate in counts per ks.

^bBest fit parameters. kT_{eff} for a neutron star atmosphere model and α for a power-law component. Both were combined in the case of source #4.

^cUnabsorbed flux (units of 10^{-13} erg cm⁻² s⁻¹) between 0.5–10 keV.

^dType of X-ray source. qNS = transient neutron star in quiescence.

*The value of the slope in parenthesis are held fixed at the value $\alpha = 1$.

Table 4. H-atmosphere spectral parameters for source #4, #9 and #5 for other known probable GC and field qNSs

Object	R_∞ (km)	kT_{eff} (eV)	d (kpc)	$N_{H,22}$	α	L_X	F_X	Ref.
XMMU 171411–293159	$10.7^{+6.3}_{-3.1}$	115^{+21}_{-16}	5.97	(0.266)	–	0.65	1.52^1	present work
XMMU 171421–292917	23^{+69}_{-10}	70^{+28}_{-20}	5.97	(0.266)	–	0.07	0.59^1	present work
XMMU 171433–292747	$11.6^{+6.3}_{-4.6}$	122^{+31}_{-45}	5.97	(0.266)	$1.2^{+0.7}_{-0.8}$	1.01	2.3^1	present work
ω Cen(ACIS)	$14.3^{+2.1}_{-2.1}$	66^{+4}_{-5}	5	(0.09)	–	0.5 ± 0.2	1.67 ± 0.67^2	1
ω Cen(EPIC)	$13.6^{+0.3}_{-0.3}$	67^{+2}_{-2}	5.3	0.09 ± 0.025	–	0.32 ± 0.02	0.95 ± 0.06^2	2
M13 (EPIC)	$12.8^{+0.4}_{-0.4}$	76^{+3}_{-3}	7.7	(0.011)	–	0.73 ± 0.06	1.03 ± 0.08^2	3
47 Tuc X5	$19.0^{+8.8}_{-7.8}$	101^{+21}_{-14}	4.85	$0.09^{+0.08}_{-0.05}$	–	1.4	$4.3^{1,*}$	4
47 Tuc X7	$14.5^{+1.8}_{-1.6}$	$105.4^{+5.6}_{-5.6}$	4.85	$0.042^{+0.018}_{-0.016}$	–	1.5	$5.3^{1,*}$	5
M 28 (#26)	$14.5^{+6.9}_{-3.8}$	90^{+30}_{-10}	5.5	0.26 ± 0.04	–	$1.2^{+0.7}_{-0.4}$	$3.35^{+1.9}_{-1.1}^3$	6
M 30 A-1	$13.4^{+4.3}_{-3.6}$	94^{+17}_{-12}	9.0 ± 0.5	$0.029^{+0.017}_{-0.012}$	–	0.71	$0.73^{1,*}$	7
NGC 6397 (U24)	4.9^{+14}_{-1}	57–92	2.5	0.1–0.26	–	0.08	$1.06^{5,*}$	8
M80 CX2	(10)	82 ± 2	$10.3^{+0.8}_{-0.7}$	$0.09^{+0.025}_{-0}$	–	0.29 ± 0.02	0.23 ± 0.02^4	9
M80 CX6	(10)	76^{+5}_{-6}	$10.3^{+0.8}_{-0.7}$	$0.22^{+0.08}_{-0.07}$	–	0.09 ± 0.01	0.07 ± 0.01^4	9
NGC 2808 C2	(12)	$81.3^{+5.3}_{-4.9}$	9.6	0.82 ± 0.40	–	0.26 ± 0.04	0.24 ± 0.04^1	10
NGC 3201 16	(10)	172^{+55}_{-42}	5.0	(1.17)	1.04 ± 0.63	0.34	$1.0^{0,*}$	11
Aql X-1	13.4^{+5}_{-4}	135^{+18}_{-12}	5	$0.35^{+0.08}_{-0.07}$	(1.0)	4.4	$14.7^{1,*}$	12
Cen X-4	$16.8^{+2.6}_{-2.6}$	59^{+6}_{-6}	1.2	(0.055)	$1.0^{+0.6}_{-0.4}$	0.17	$0.6^{1,*,v}$	13
^a 4U 2129+47	$9.3^{+7.8}_{-4.6}$	60^{+15}_{-11}	1.5	(0.28)	–	$0.07^{+0.15}_{-0.03}$	$2.4^{+5.1}_{-1.0}^6$	14
^a 4U 2129+47	$16^{+11.0}_{-6.40}$	80^{+19}_{-15}	6.0	(0.17)	–	$0.56^{+0.12}_{-0.3}$	$1.3^{+0.3}_{-0.7}^6$	14
^a 4U 1608-522	$12.3^{+5.9}_{-3.5}$	130^{+20}_{-20}	3.6	(0.8)	–	0.83 ± 0.42	5.4 ± 2.7^1	15
^a 4U 1608-522	65^{+47}_{-26}	80^{+15}_{-12}	3.6	(1.5)	–	0.73 ± 0.47	4.7 ± 3.0^1	15

Note. — For the qLMXBs of the present work, the mass was kept fixed to $1.4 M_\odot$. As mentioned in the text, the tabulated model of the neutron star atmosphere was used for XMMU 171411–293159 and XMMU 171421–292917 while a `nsa+PL` model was used to fit the spectrum of XMMU 171433–292747. The top part of the table contains GC qLMXBs while the second part only shows the parameters of field qLMXBs. The inferred radius is measured using the distance to the GC quoted in the text. Previously measured values of the radius have been converted from R to R_∞ , the projected radius. Error bars are 90 per cent confidence. Values in parenthesis are held fixed. The unabsorbed X-ray luminosity L_X and flux F_X are expressed in units of $10^{33} \text{ erg s}^{-1}$ and $10^{-13} \text{ erg cm}^{-2} \text{ s}^{-1}$, respectively, both in X-ray bands listed below.

^aDifferent assumed values of D and/or N_H .

⁰0.2–10 keV band.

¹0.5–10 keV band.

²0.1–5 keV band.

³0.5–8 keV band.

⁴0.5–6 keV band.

⁵0.5–2.5 keV band.

⁶0.5–3.0 keV band.

*No error was provided by the authors.

^vIndicates that the source flux varies.

Note. — References: 1, Rutledge et al. (2002a); 2, Gendre et al. (2003b); 3, Gendre et al. (2003a); 4, Heinke et al. (2003b); 5, Heinke et al. (2006); 6, Becker et al. (2003); 7, Lugger et al. (2007); 8, Grindlay et al. (2001b); 9, Heinke et al. (2003a); 10, Servillat et al. (2008); 11, Webb et al. (2006) 12, Rutledge et al. (2001a); 13, Rutledge et al. (2001b); 14, Rutledge et al. (2000); 15, Rutledge et al. (1999)

Table 5. Difference in the Luminosities between the *ROSAT* and the current *XMM-Newton* observations

ID	XMM-pn		ID _{R94}	ROSAT	
	$kT_{\text{eff, BB}}$ ^a	ECF ^b		Counts predicted ^c	Counts Observed ^d
4	260±30	0.0935±0.0015	A	20.7±1.5	15
5	170±30	0.0855±0.0065	B	3.9±0.9	7
9	200±30	0.090±0.002	C	11.4±1.0	17
-	-	0.062	D	<1.8	14

Note. — For source D, due to the non detection, a 3σ upper limit is calculated.

^aThe $kT_{\text{eff, BB}}$ is the black-body effective temperature, from spectral fits to the present XMM data.

^bThe energy-conversion-factor (ECF) is the number of ROSAT/HRI counts per XMM count for each source, which depends on $kT_{\text{eff, BB}}$ and N_H (assumed to be $N_{H,22} = 0.266$). For R94 source D, undetected in the present observation, an absorbed thermal bremsstrahlung spectrum with $kT = 3$ keV is assumed.

^cThe total counts predicted for the R94 observation based on the present XMM observation, using the source spectrum measured here; the predicted HRI countrate from WebPIMMS; and the ROSAT/HRI observation duration of 5030 sec.

^dThe total number of source counts from ROSAT/HRI observation (R94), corrected for observation at the HRI centre (that is, after subtracting background counts, correcting for vignetting, quantum efficiency and scattering). The uncertainty in this number is not given by R94.

Table 6. Distance from the core of the candidate qLMXBs and other known or probable qNSs in GCs.

Object Name	d_c (arcmin)	r_c (arcmin)	Δ/r_c	Ref.
XMMU 171411–293159	6.7	0.21	31.8	0
XMMU 171433–292747	0.17	0.21	0.79	0
XMMU 171421–292917	3.2	0.21	15.2	0
ω Cen	4.38	2.58	1.7	1
M13	0.74	0.78	0.95	2,10
47 Tuc X7	< 0.37	0.38	< 1.5	3
47 Tuc X5	< 0.37	0.38	< 1.5	3
M 28 (#26)	0.05	0.24	0.21	4,10
M 30 A-1	0.03	0.06	0.5	5,10
NGC 6397 (U24) ^{cc}	0.34	0.05	6.8	6,10
M80 CX2	0.063	0.15	0.42	7,10
M80 CX6	0.324	0.15	2.2	7,10
NGC 2808 C2	0.08	0.26	0.31	8,10
NGC 3201 16	5.8	1.43	4.1	9,10

Note. — This table is a compilation of the positional information of known qLMXBs and candidates qLMXBs in GCs. The columns, from left to right, are the object name (or the GC hosting the qLMXB), the distance of the qLMXB from the optical centre of the GC (in arcminutes), the core radius of the GC (in arcminutes) and the distance of the qLMXB from the optical centre of the GC in units of core radii. References : 0, present work; 1, Rutledge et al. (2002a); 2, Gendre et al. (2003a); 3, Heinke et al. (2003b); 4, Becker et al. (2003); 5, Lugger et al. (2007); 6, Grindlay et al. (2001b); 7, Heinke et al. (2003a); 8, Servillat et al. (2008); 9, Webb et al. (2006); 10, Harris (1996), for the core radii values.

^{cc}NGC 6397 is a core collapsed star cluster.